A Novel Method of Improving EEG Signals for BCI Classification

by

Christiaan Burger

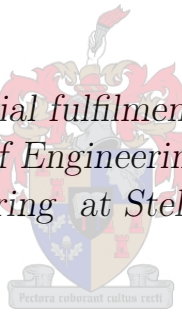

Thesis presented in partial fulfilment of the requirements for the degree of Master of Engineering (Mechatronic) in the Faculty of Engineering at Stellenbosch University

Supervisor: Dr. D.J. van den Heever

December 2014

Declaration

By submitting this thesis electronically, I declare that the entirety of the work contained therein is my own, original work, that I am the sole author thereof (save to the extent explicitly otherwise stated), that reproduction and publication thereof by Stellenbosch University will not infringe any third party rights and that I have not previously in its entirety or in part submitted it for obtaining any qualification.

Date: .....

Abstract

A Novel Method of Improving EEG Signals for BCI Classification

C. Burger

Thesis: MScEng (Mech)

December 2014

Muscular dystrophy, spinal cord injury, or amyotrophic lateral sclerosis (ALS) are injuries and disorders that disrupts the neuromuscular channels of the human body thus prohibiting the brain from controlling the body. Brain computer interface (BCI) allows individuals to bypass the neuromuscular channels and interact with the environment using the brain. The system relies on the user manipulating his neural activity in order to control an external device. Electroencephalography (EEG) is a cheap, non-invasive, real time acquisition device used in BCI applications to record neural activity. However, noise, known as artifacts, can contaminate the recording, thus distorting the true neural activity. Eye blinks are a common source of artifacts present in EEG recordings. Due to its large amplitude it greatly distorts the EEG data making it difficult to interpret data for BCI applications. This study proposes a new combination of techniques to detect and correct eye blink artifacts to improve the quality of EEG for BCI applications.

Independent component analysis (ICA) is used to separate the EEG signals into independent source components. The source component containing eye blink artifacts are corrected by detecting each eye blink within the source component and using a trained wavelet neural network (WNN) to correct only a segment of the source component containing the eye blink artifact. Afterwards, the EEG is reconstructed without distorting or removing the source component. The results show a 91.1% detection rate and a 97.9% correction rate for all detected eye blinks. Furthermore for channels located over the frontal lobe, eye blink artifacts are corrected preserving the neural activity. The novel combination overall reduces EEG information lost, when compared to existing literature, and is a step towards improving EEG pre-processing in order to provide cleaner EEG data for BCI applications.

Uittreksel

'n Nuwe Metode om EEG Seine vir BCI Klassifikasie te verbeter

("A Novel Method of Improving EEG Signals for BCI Classification")

C. Burger

Tesis: MScIng (Meg)

Desember 2014

Spierdistrofie, 'n rugmurgbesering, of amiotrofiese laterale sklerose (ALS) is beserings en steurnisse wat die neuromuskulêre kanale van die menslike liggaam ontwrig en dus verhoed dat die brein die liggaam beheer. 'n Breinrekenaarkoppelvlak laat toe dat die neuromuskulêre kanale omlei word en op die omgewing reageer deur die brein. Die BCI-stelsel vertrou op die gebruiker wat sy eie senuwee-aktiwiteit manipuleer om sodoende 'n eksterne toestel te beheer. Elektro-enkefalografie (EEG) is 'n goedkoop, nie-indringende, intydse dataverkrygingstoestel wat gebruik word in BCI toepassings. Nie net senuwee aktiwiteit nie, maar ook geraas , bekend as artefakte word opgeneem, wat dus die ware senuwee aktiwiteit versteur. Oogknip artefakte is een van die algemene artefakte wat teenwoordig is in EEG opnames. Die groot omvang van hierdie artefakte verwring die EEG data wat dit moeilik maak om die data te ontleed vir BCI toepassings. Die studie stel 'n nuwe kombinasie tegnieke voor wat oogknip artefakte waarneem en regstel om sodoende die kwaliteit van 'n EEG vir BCI toepassings te verbeter.

Onafhanklike onderdeel analise (Independent component analysis (ICA)) word gebruik om die EEG seine te skei na onafhanklike bron-komponente. Die bron-komponent wat oogknip artefakte bevat word reggestel binne die komponent en gebruik 'n ervare/geoefende golfsenuwee-netwerk om slegs 'n deel van die komponent wat die oogknip artefak bevat reg te stel. Daarna word die EEG hervorm sonder verwringing of om die bron-komponent te verwyder. Die resultate toon 'n 91.1% opsporingskoers en 'n 97.9% regstellingskoers vir alle waarneembare oogknippe. Oogknip artefakte in kanale op die voorste lob word reggestel en behou die senuwee aktiwiteit wat die oorhoofse EEG kwaliteit vir BCI toepassings verhoog.

Acknowledgements

First and foremost I want to thank my supervisor Dr. David J. van den Heever for his patience, guidance, and support throughout the course of this thesis.

I am grateful to all my friends and office colleagues for supporting and keeping me motivated when things appeared grim. I thank my parents and Nedine for their support, their love, and them believing in me. For without their support this thesis would never have been possible.

Lastly I thank the National Research Foundation (NRF) for their financial contribution to the thesis. The financial assistance of NRF towards this research is hereby acknowledged. Opinions expressed and conclusions arrived at, are those of the author and are not necessarily to be attributed to the NRF.

Contents

List of Figures

List of Tables

Nomenclature

Abbreviations

ALS	Amyotrophic Lateral Sclerosis
ANN	Artificial Neural Network
AP	Action Potential
BBCI	Berlin Brain Computer Interface
BCI	Brain Computer Interface
BSS	Blind Source Separation
CNS	Central Nervous System
CWT	Continuous Wavelet Transform
DWT	Discrete Wavelet Transform
EEG	Electroencephalography
EKG	Electrocardiogram
EPSP	Excitatory Postsynaptic Potential
ERD	Event-Related Synchronization
ERS	Event-Related Desynchronization
FC	Frequency Correlation
FIR	Finite Impulse Response
fMRI	Functional Magnetic Resonance Imaging
ICA	Independent Component Analysis
IPSP	Inhibitory Postsynaptic Potential
MEG	Magnetoencephalography
NG	Non-Gaussian
NS	Non-Stationary
PET	Positron Emission Tomography
PNS	Peripheral Nervous System
PSD	Power Spectral Density
RMSE	Root Mean Square Error
SCP	Slow Cortical Potential
SD	Spectral Density

SPECT	Single Photon Emission Computerized Tomography
SSVEP	Steady-state Visual Evoked Potential
STFT	Short Time Fourier Transform
VEP	Visual Evoked Potential
WNN	Wavelet Neural Network

Symbols

$\mathbf{A}$	Mixing Matrix	[ ]
$\widetilde{\mathbf{A}}$	Uncorrelated Mixing Matrix	[ ]
a	Filter Parameters	[ ]
b	Filter Parameters	[ ]
c	Wavelet Coefficients	[ ]
$\mathbf{D}$	Eigenvalues Matrix	[ ]
E	Global Error	[ ]
f_0	Center Frequency	[ ]
$\triangle f$	Frequency Bandwidth	[ ]
G	Network Output	[ ]
g	Perceptron Output	[ ]
H	Entropy	[ ]
J	Negentropy	[ ]
$\mathbf{k}$	Observed Vector	[ ]
$\widetilde{\mathbf{k}}$	Uncorrelated Observed Vector	[ ]
L	Heaviside Function	[ ]
N	Total Number of Weigths	[ ]
n	Total Number of Parameters	[ ]
$\mathbf{n}$	Noise Vector	[ ]
O	Total Blink Artifacts	[ ]
OA	Blink Artifact	[ ]
P	Probability	[ ]
Q	Filter Frequency Spectrum	[ ]
q	Filter Coefficients	[ ]
R	Total Number of Patterns	[ ]
s	Scaling Parameter	[ ]
$\mathbf{s}$	Source Vector	[ ]
TH	Threshold	[ ]
t	Time	[s]

U	Filter Parameters	[ ]
u	Translation Parameter	[ ]
W	Unmixing Matrix	[ ]
$\mathbf{w}$	Unmixing Vector	[ ]
X	Network Input	[ ]
x	Perceptron Input	[ ]
y	Random Variable	[ ]
δ	Update Value	[ ]
ϵ	Learning Rate	[ ]
η	Step Size	[ ]
Λ	Eigenvector Matrix	[ ]
Ψ	Wavelet	[ ]
ω	Perceptron Weight	[ ]

Superscripts

T	Transpose	[ ]

Subscripts

e	Blink Artifact Index	[ ]
$gaus$	Gaussian	[ ]
i, j	Index	[ ]
MAX	Maximum	[ ]
m	Mixing Matrix Size	[ ]
TH	Threshold	[ ]

Chapter 1

Introduction

1.1 Motivation

Disorders such as amyotrophic lateral sclerosis (ALS), brain or spinal cord injury, muscular dystrophies, multiple sclerosis and various other diseases disrupts the neuromuscular channels. This makes the brain incapable of controlling parts of the human body [1]. Some severe cases occur such as loss of muscle control (limb control or respiration) or patients are completely locked within their bodies, unable to communicate.

Electroencephalography (EEG) is the measurement of the brain's electrical neural activity that was discovered by Hans Berger in 1920 [2]. EEG is widely used in clinical settings for brain activity monitoring, characterizing seizures and has many research applications in neuroscience, cognitive science, psychology, psychophysiology, and as a diagnostic tool. As time passed, people started to consider that there are other possible uses for EEG, uses such as deciphering thoughts or to control devices using your thoughts. After approximately a hundred years the first research on brain computer interface (BCI) was conducted by Jacques Vidal [2].

BCI, also known as brain-machine interfacing (BMI), is the link that is formed between the human brain and the physical world without any physical contact. It allows the user to manipulate their neural activity to control an external device. The primary focus of BCI is to create a communications tool for those affected by the previously mentioned conditions, which allows them to cope in today's society without disabilities as a disadvantage. However BCI has a wide range of other applications including video games and virtual reality [3], internet browsing [4], creative expressions [5] etc.

The full potential of EEG has not been fully utilised due to misinterpretation of EEG data which in the past discredited EEG research [6] and can lead

to inaccurate BCI systems. It is important to understand that the EEG data that each of the electrodes record is not just the neural activity directly under it, but an accumulation of different neural and electrical activities. Other activities such as eye blinks, eye movements, heartbeat, and respiration produces electrical activity that distorts the true EEG activity. These electrical activities that distort the true EEG are known as artifacts [1; 7; 8]. Eye blinks, the most prominent artifact, can generate an amplitude 10 to 100 times larger than cerebral activity thus distorting most of the frontal electrodes [2; 9].

Currently there exists many different techniques used to remove eye blink artifacts to improve the quality of EEG. One simple method is restricting eye blinking by focusing on a single point. This however is difficult for an individual to do, especially for infants. Independent component analysis (ICA) uses blind source separation to separate the EEG into separate independent sources then removes the artifact sources and recombine all the sources creating an artifact free EEG [10]. The sources generated are however not the true sources but an estimate, a combination of artifact and neural sources. As a result, when the artifact source is removed, underlying neural activity is also removed reducing EEG quality. High pass filters and epoch rejection both work on the basis of rejecting a desired range of data, whether data in a lower frequency band or time period [11]. Eye blink artifacts are removed but a portion of the EEG is also lost thus lowering EEG quality.

1.2 Literature Review

Research predominantly focuses on the sensorimotor cortex, which can be activated by imagining motor functions, for BCI applications. Vansteensel et al. [13] analysed whether it was possible to use the cognitive control network for a simple cursor control BCI application instead of the sorimotor cortex. The left anterior dorsolateral prefrontal cortex (DLPFC), the cognitive control network which regulates the flow of information in the brain, was chosen based on its involvement in deliberate processing of information. Using functional magnetic resonance imaging (fMRI) three subjects with intractable epilepsy were scanned while completing task in order to localize functionally relevant regions. Afterwards electrocorticographic (ECoG) sensors were implanted with the location of the ECoG grid based on clinical considerations. For testing, a 1-dimentional 2-target control setup was used where a single electrode and frequency band was selected to measure the power, voluntarily modulated, to move the cursor. All three subjects produced 80 % correct hits for the cursor control test thus, Vansteensel et al. [13] proved that the DLPFC is suitable for EGoC-BCI applications as well as clinical research applications.

Research regarding BCI are very susceptible to noise which can alter the final

results obtained. Eye blink artifacts are the most common artifacts present and for the BCI research discussed above they are severe, thus methods exist to remove or correct artifacts. Repovs [11] discusses different techniques that are available to remove artifacts. Artifacts fixed in a set frequency band can be removed by passing the data through a series of filters. However, underlying EEG data present in the frequency band can be lost. Subtraction by linear regression can be used to remove ocular artifacts. The source of the artifact is recorded and multiplied by a constant and the resulting value is subtracted from the desired EEG channel recording data. The constant is dependent on the distance between the artifact source and the channel that needs correction. The most common method of removing artifacts is through blind source separation. The EEG data is decomposed into independent source components, using ICA, and the source component containing the artifacts are then removed. The source components aren't a true estimate of each source generating artifact and EEG activity but, rather an estimate. Thus by removing the artifact source component, underlying EEG data present in the source component is also lost.

Venkataramanan et al. [14] analysed a novel and simple technique that detects and subsequently removes ocular artifacts using a high order Haar wavelet. The contaminated EEG data was decomposed using a Haar wavelet up to 8 levels which produces 8 detailed frequency bands and an approximate frequency band. The approximate frequency band yields a step function whose falling edge accurately detects an eye closing. Furthermore, rising edge accurately detects an eye opening. This method is used to detect the location of the eye blink with the EEG data. Extending this technique allows the artifact to be filtered out by zeroing the portion of the reconstructed approximate frequency band.

Nguyen et al. [15] proposed to combine wavelet transforms with neural networking to correct ocular artifacts. The data is decomposed using a coif3 wavelet up to level six and the lowest three frequency bands are evaluated by the neural network and corrected if any artifacts are present. Using a simulation model provided by [16] the artifact free data was generated and impregnated with ocular artifacts extracted from EEG data. The simulated data was used to train and quantitatively asses the combined correction accuracy of the wavelet transform and the wavelet neural network. The combination was very successful however, due to some low frequency information being present in the ocular artifacts during its extraction for the simulated data, the combined system overcorrects low frequency information during artifact correction.

Li et al. [12] analysed a novel method which automatically detects and removes ocular artifacts by combining discrete wavelet transform (DWT) and ICA. Each channel of the recording was decomposed up to 3 levels using Sym8

mother wavelet where the coefficients were ranked in order and placed in a vector. Independent sources were determined by applying ICA, based on negentropy criteria, to the raked coefficient vectors. The artifact independent source component was identified by comparing each independent source component wavelet coefficient vector with the wavelet coefficient vector of the reference ocular artifact channel using the angle cosine criteria. The identified ocular artifact component wavelet coefficients were zeroed and the remainder of the components were recombined create ocular artefact free EEG. The combination was very successful and resulted in a powerful noise immunity and fast convergence rate for online preprocessing.

From the research and methods described above it is observed that there exist many methods or combination of methods that can be utilised for artifact removal however, with each method, underlying EEG data can be lost. Combinations of different methods have already been researched (for example, DWT and ICA) however the method the combination is applied in order to remove artifacts is different. The thesis proposes a novel combination of processing methods to minimise the underlying data loss as well as to improve on the method proposed by [15].

1.3 Objectives

EEG is a core part of BCI thus it is important that EEG signals are recorded with as little noise as possible. However, the body produces noise that contaminate EEG data, such as eye blinks (see Section 1.1). Thus, it is important to remove the noise to improve the quality of EEG. The goal of the thesis is to implement an algorithm that, instead of rejecting the components containing the eye blink artifacts, corrects the components, reducing the amount of neural activity lost. This goal is divided into primary and secondary objectives to simplify the design process.

- Primary Objective
  - Develop an algorithm that can automatically detect and isolate eye blinks.
  - Develop an algorithm that can correct eye blinks with minimal neural activity loss.
- Secondary Objective
  - Determine the severity of the impact eye blinks have on EEG channels (C_3 and C_4) located above the motor cortex.

1.4 Thesis Structure

This thesis is structured as follows. Chapter 2 describes the basic information concerning the generation of electrical activity within the brain, EEG, artifacts disrupting EEG, and BCI. Chapter 3 discusses the fundamental information of wavelet analysis and decomposition, ICA, and neural networks regarding the methods used in the detecting and correcting algorithm. Chapter 4 briefly discusses the setup used to simulate EEG data used during the algorithms' training and testing. In chapter 5 the data sets used for testing is described then the complete process, detecting and correcting eye blinks, is discussed starting at the input EEG and ending with artifact free EEG. Afterwards the two main components (detecting and correcting artifacts) is discussed separately in detail followed by the description of the testing procedures. Chapter 6 presents the results obtained and the assessment of the results as well as comparison to previous methods are discussed in chapter 7. The thesis ends with chapter 8 in which we discuss the objectives achieved.

Chapter 2

Backgound

This section gives a brief overview on the anatomy of the brain and the sources behind its electrical activities. This is followed by a description of EEG and the neural activity that is recorded. Finally this section will look at the type of artifacts that influence and degrades the quality of EEG and how it is implemented in BCI.

2.1 The Brain

In order to properly interpret EEG results a thorough understanding is required of the anatomy and functional areas of the brain. The human brain is separated into three sections; the forebrain, midbrain, and hindbrain. The forebrain includes the telencephalon (cerebrum and basal ganglia) and diencephalon (thalamus, hypothalamus, and subthalamus), the midbrain includes the corpora quadrigemina and the hindbrain includes the metenchaphalon (pons and cerebellum) and myelencephalon (medulla oblongata) [8; 17; 18]. The cerebrum is the largest part of the brain and consists of a left and right hemisphere interconnected by the corpus callosum. Both hemispheres are covered in a 2-5mm thick layer known as gray matter (cerebral cortex) which consists of folds (gyri) and groves (sulci) that increases the surface area. Due to the high density of neurons in the cerebral cortex and the close proximity it has to the recording electrodes, it is the focus of EEG studies [8].

As seen in Figure 2.1 the cerebrum is naturally separated into five lobes; the frontal lobe, parietal lobe, temporal lobe, occipital lobe, and the insula (not seen in surface views). The frontal lobe is separated from the parietal lobe by a deep sulcus known as the central sulcus. The lateral sulcus separates the frontal lobe from the temporal lobe and the occipital lobe is separated from the parietal lobe by the parieto-occipital sulcus [17].

The cerebrum is the source of higher brain function such as intellect, conscious

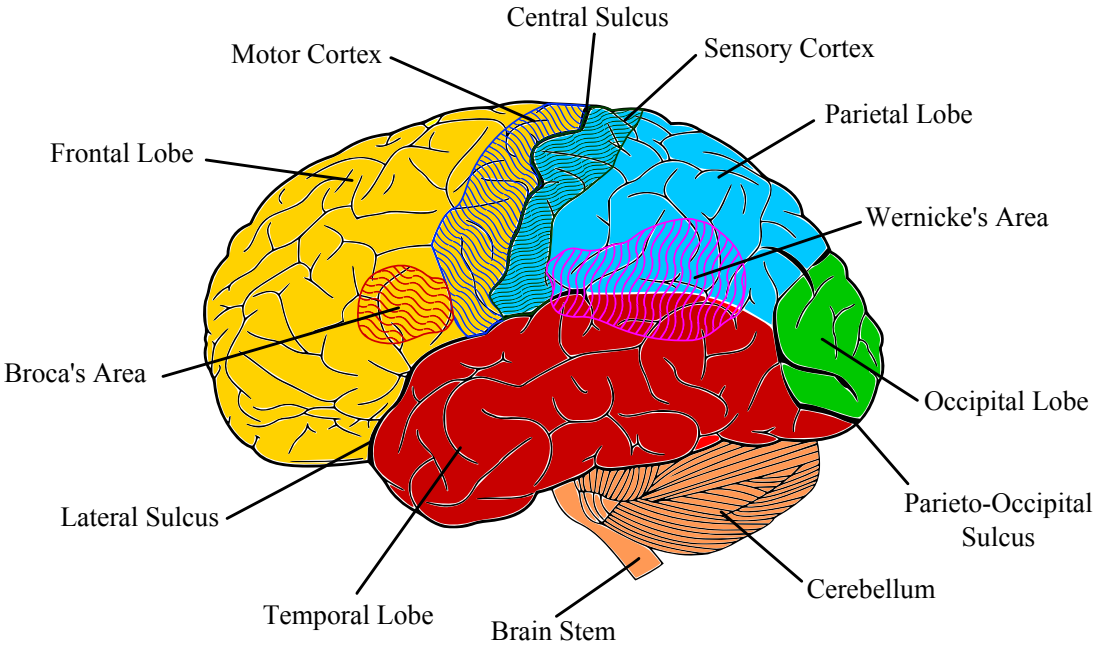

Figure 2.1: Surface anatomy of the brains left hemisphere (adapted from [17]).

thought, complex movements, speech, and sensation [17]. The primary motor cortex, situated anterior to the central sulcus (posterior of the frontal lobe) and the primary sensory cortex, situated posterior to the central sulcus (anterior of the parietal lobe) are responsible for the control of the skeletal muscles and the interpretation of the sensory information such as touch [8; 17]. The premotor cortex, situated anterior to the primary motor cortex, is associated with coordinated learned movement whereas the visual cortex, situated posteriorly in the occipital lobe, interprets visual stimuli.

As mentioned before, the brain is divided into a left and right hemisphere. The brain makes use of contralateral control, the arrangement of motor and sensory fibres that results in contralateral control of body portions by the motor cortex [19]. Logical or language functions are primarily located in the left hemisphere, which is the most predominant hemisphere. The expressive speech area (Broca's area), responsible for the production of language, and the receptive speech area (Wernicke's area), responsible for the understanding of language, is interconnected so that the production of languages makes sense. The right hemisphere, specialized in spatial comprehension (creativeness), allows the interpretation of emotion and melody in language as well as expression [18].

2.2 Neural Activity of the Brain

The human body interacts with the physical world by using its nervous system. The nervous system consists of two categories, the central nervous system (CNS) and the peripheral nervous system (PNS). The CNS is the system containing all the nerves that are situated within the spinal cord and brain. Its function is to process the information it receives from, and control all parts of the body. The PNS consists of all the nerves that are situated outside of the brain and spinal cord. Its function is to connect the CNS to the limbs and organs [1; 17; 18].

The basic building blocks of the CNS are nerve cells (neurons) and glia cells, situated between neurons. Each nerve cell consists of an axon, dendrites and cell body as seen in Figure 2.2(a). The nerve cells transmit information throughout the body in the form of electrical impulses. The axon acts as the pathway that conducts the electrical impulse, whereas the dendrites, connected to either axons or other dendrites, distributes the impulse to another nerve cell [2]. Different electrical impulses can occur within a nerve cell. When an action potential (AP) stimulates excitatory synapses an excitatory postsynaptic potential (EPSP) is produced. An inhibitory postsynaptic potential (IPSP), which indicates hyperpolarization, is produced when an inhibitory synapse is stimulated by an AP [2; 17; 20]. EPSP or IPSP is generated within the following nerve cell, as seen in Figure 2.2(b), by the active postsynaptic current. After either EPSP or IPSP has occurred, a potential along the nerve cell is produced due to a concentration difference of cations (positively charged ions) or anions (negatively charged ions) between the outside and inside of the nerve cell. Primary transmembranous currents, caused by a potential difference along nerve cells, generates extracellular currents which are responsible for the generation of field potentials [2; 20].

The information transferred through the nerve cell are in the form of APs. An AP is caused by an exchange of ions that diffuse across the neuron membrane thus creating a temporary change in the membrane potential. The exchange of ions is caused by an EPSP that must surpass a threshold potential to initiate an AP. In order to surpass the threshold more than one presynaptic neuron must produce an EPSP at the same time [21], as seen in Figure 2.3(a). During the exchange of ions the membrane potential rapidly depolarizes thus becoming more positive, creating a spike. To return the membrane potential back to equilibrium, it repolarises thus becoming more negative and returning to its original membrane potential known as the resting membrane potential [2; 17; 21].

Looking only at one neuron, Figure 2.3(b), shows the AP spike that is produced when a neuron is stimulated. The predominant ions that are involved in

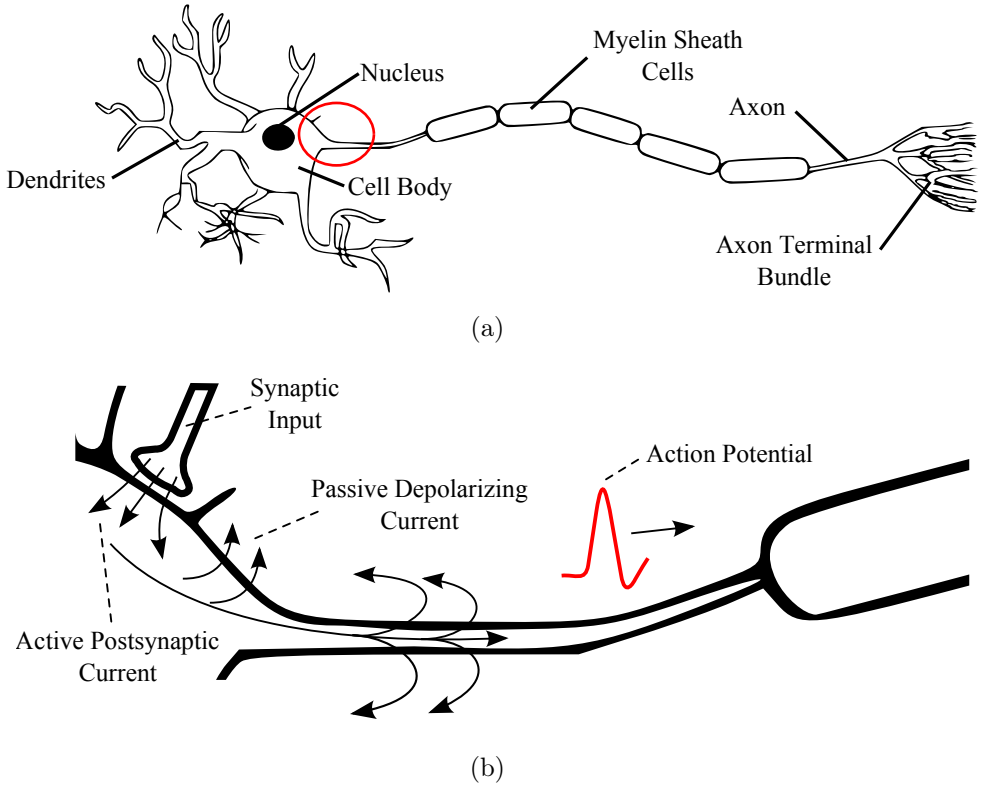

Figure 2.2: CNS nerve cells a) anatomy and b) electrical impulse generation (adapted from [2]).

the spike of the AP are Na^+ and K^+. When the neuron is stimulated, rapid depolarization occurs and Na^+ voltage gated channels (active when stimulated with a potential difference) open and allows Na^+ to diffuse into the neuron cell membrane, increasing its potential. If this potential reaches the threshold potential (-55 mV) then more Na^+ voltage gated channels open and allows more Na^+ to diffuse and causes the membrane potential to increase to +30 mV[2]. Before reaching the peak the Na^+ voltage gated channels become inactive and Na^+ stops diffusing. The K^+ voltage gated channels open and K^+ starts to diffuse outwards of the cell membrane thus lowering the membrane potential. This process is known as repolarisation. The Na^+ voltage gated channels become active again and Na+ starts to diffuse again so that equilibrium (membrane resting potential) can be achieved[2].

During the process to reach equilibrium, the repolarisation overshoots the resting membrane potential (see Figure 2.3(b)). This is known as hyperpolarisation. Hyperpolarisation is a safety measure to ensure that the neuron does not receive another stimulus causing another AP in the opposite direction [2]. After hyperpolarisation the membrane potential returns to its resting membrane potential (-70 mV). The entire process including the recovery period

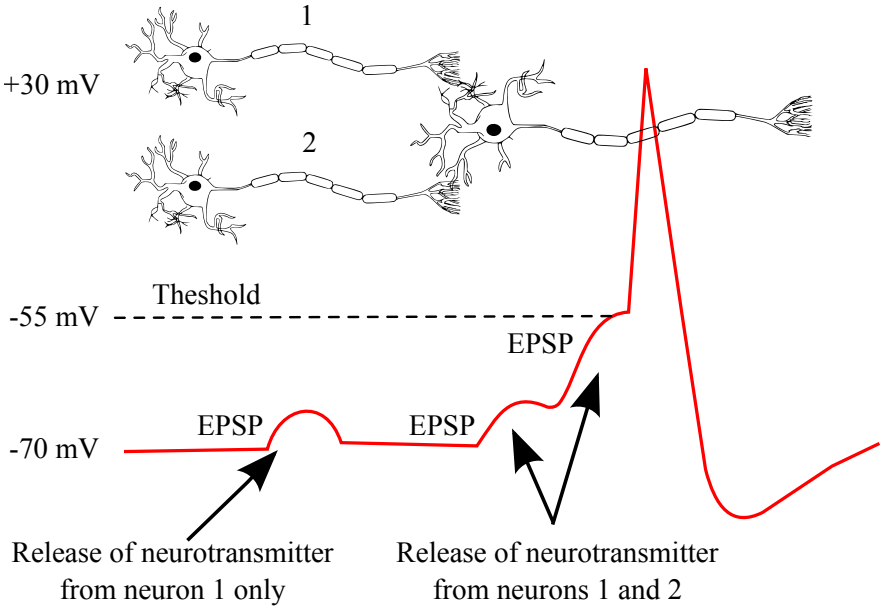

(a)

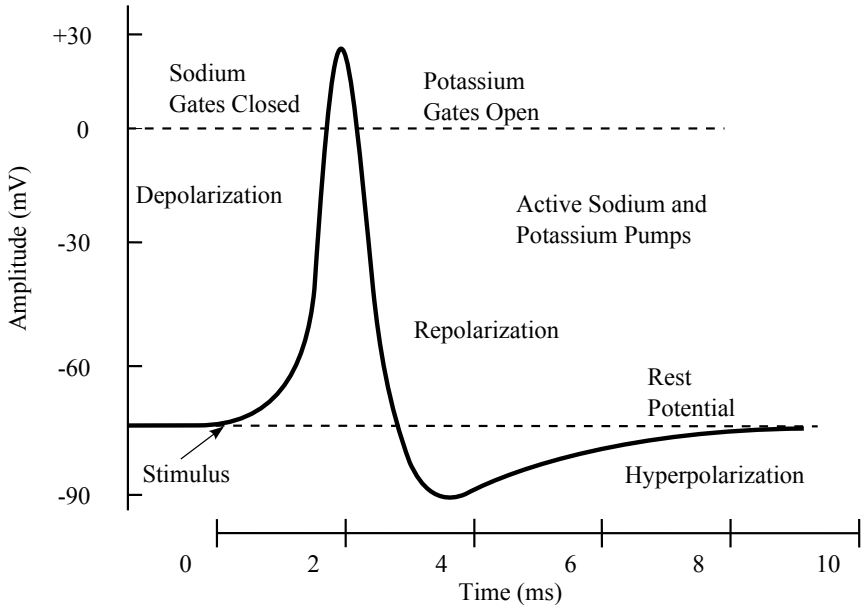

(b)

Figure 2.3: Action potentials a)threshold limit and b) ion exchange during generation (adapted from [2; 17]).

before another AP is generated, lasts 8ms [21].

2.3 EEG Basics

The neurons within the brain produces APs that contribute to the generation of neural activity recorded by EEG. There are 10^{10} to 10^{11} neurons within the brain and it is the summation of their activities that produces the neural activity [8]. During the excitation of tens of thousands of pyramidal neurons, a current flow is generated which in turn produces electrical dipoles between the body of the neuron and the dendrites. EEG is a technique used to measure the electrical dipole, between 2 different cerebral locations, generated by the cerebral cortex [7; 22] (see Figure 2.4). However, the signals recorded by EEG electrodes are not only the neural activity of the source situated below the electrode, but a summation of neural activity that is conducted from different parts of the brain.

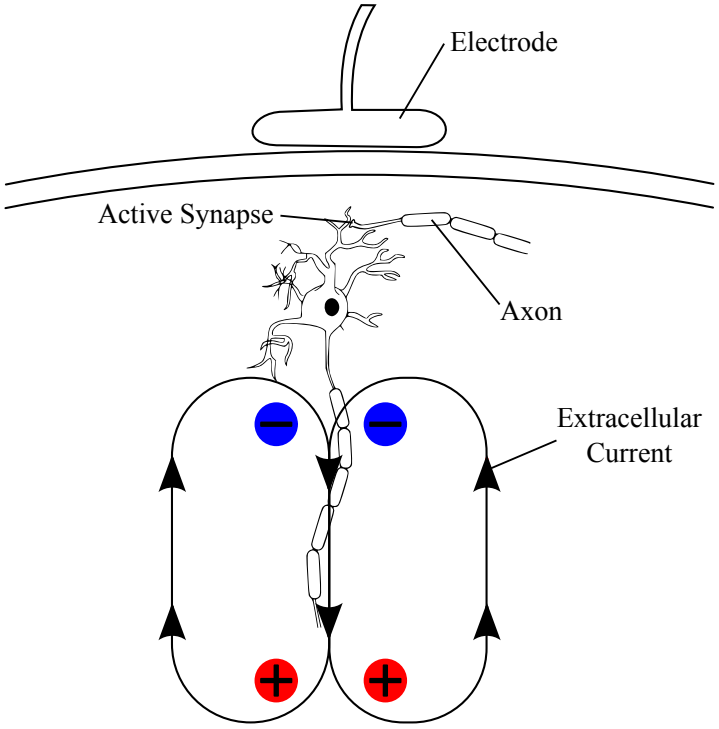

Figure 2.4: Electrical dipole measured by EEG electrode.

EEG is a non-invasive procedure (does not require any device to enter the body) that uses electrodes to measure the neural activity. An average electrode usually consist of 1 to 3 mm diameter Ag-AgCl disks [7] and is placed directly on the scalp. Different type of electrodes exists, such as;

- disposable (gel-less, and pre-gelled);
- reusable disc electrodes (gold, silver, stainless steel, or tin);
- headbands and electrode caps;
- saline-based electrodes.

Montage refers to the display characteristics of the EEG data on a screen or paper. The display characteristics include order and channels displayed as well as recording techniques (electrode referencing) styles used [23]. Two distinct recording techniques are used, known as bipolar and referential montage, but there does exist some overlap between the two techniques. Bipolar montage is a technique that determines the voltage difference between adjacent electrodes, but due to the adjacent electrodes' close proximity to one another, information is lost [23]. Referential montage compares all the electrodes on the scalp to a singular reference electrode. The location of the reference electrode can be chosen so that it has a "neutral" voltage. However, in practice if it is attached to an electrical ground the resulting tracing would be full of noise, thus it is attached to the body that has the least noise [23]. In this study, the referential montage is used due to the advantage it has over bipolar montage.

The International Federation of Societies for Electroencephalography and Clinical Neurophysiology introduced the conventional electrode placement, also known as the 10-20 system [24]. Figure 2.5(a) shows the 10-20 placements for 21 electrodes where channel F_z is placed on the forehead and channel P_z at the back. For example, if the right and left finger movement is monitored, electrodes C_3 and C_4 will be used, respectively. The earlobe electrodes (A1 and A2), not shown, are often used as reference electrodes. In order to record a more detailed EEG the 10-5 international system was created where more electrodes were placed on the scalp of the subject [24]. Figure 2.5(b) shows an example of the Geodesic sensor net with 128 channels where channel 17 is placed on the forehead and channel 82 at the back and C_z acts as the reference electrode. The Geodesic sensor net still contains the electrode locations of the 10-20 system. Channel 37, 105, and 16 of the Geodesic net is the equivalence of channels C_3, C_4, and F_z.

During the recording of EEG signals it is observed that these signals have certain characteristics. These characteristics change as a person ages as well as the state the person is in (sleeping or wakefulness)[2]. Due to these characteristics, brain waves can be broken up into six categories. These 6 categories are called alpha (α), theta (θ), beta (β), delta (δ), gamma (γ), and mu (μ) and represent a band of frequencies [2; 26]. Table 2.1 shows the frequency range of each category as well as some of the mental functions that are confirmed roles

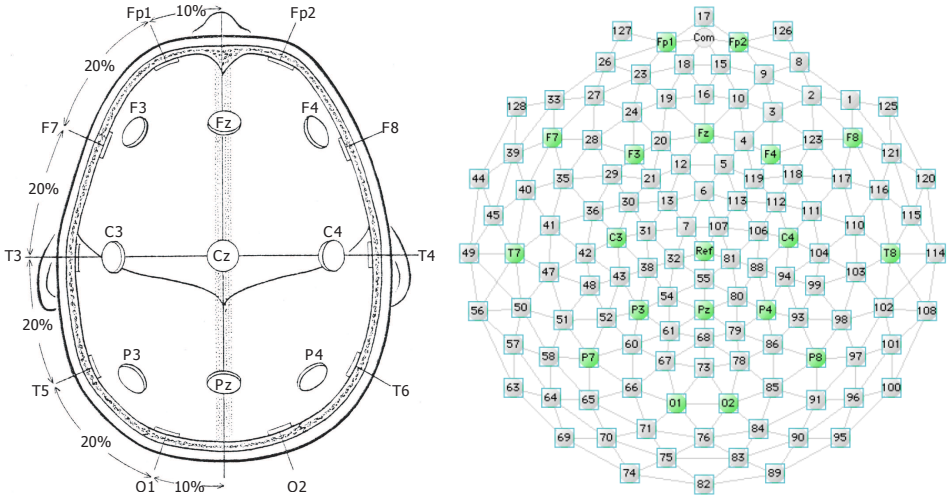

(a) (b)

Figure 2.5: Electrode location for a) 10-20 international standard [24] and b) 10-5 international standard [25].

of the frequency range.

Table 2.1: Frequency bands of brain activity

Band	**Frequency (Hz)**	**Location**	**Mental State**
Delta (δ)	4	May be wide spread.	Deep sleep; lack of attention [2; 27].
Theta (θ)	4-8	Involve many lobes.	Drowsiness; inspiration; deep meditation, emotional stress [2; 26].
Alpha (α)	8-13	Usually involves entire lobe.	Relaxation; eyes closed [2; 7; 27; 26].
Beta (β)	13-30	Frontal and central regions.	Active thinking; solving problems; focus [2; 27; 26].
Gamma (γ)	30-100	Somatosensory cortex.	Reflect mechanism of consciousness [27; 26].
Mu (μ)	8-13	Motor cortex.	Suppression during motor activity [26].

There exist many different techniques that measure the brain's activity. Functional magnetic resonance imaging (fMRI), positron emission tomography (PET), and single photon emission computerized tomography (SPECT) measure secondary functions such as metabolism or the change in oxygenation, blood volume, and flow [2; 28]. This allows these techniques to measure activity in the entire brain volume, but due to the hemodynamic lag (the time it takes for blood-oxygen levels to rise) these techniques have a low temporal resolution of 1-6 s [28; 29]. EEG, the measurement of the electrical activity of the brain, and magnetoecncephalography (MEG), measurement of the magnetic fields produced by the electrical activity of the brain, can only measure surface activity that takes place closest to the scalp. However, EEG and MEG provides high temporal resolution up to and including 1 ms [29] which makes it the ideal measuring techniques for analysing brain function. Magnetic fields are less distorted by the scalp than electrical fields, thus MEG has a higher spatial resolution than EEG. However, MEG can only detect tangential components of a current source in the brain where EEG can detect both tangential and radial components [29; 22].

EEG is mainly used in research as a non-invasive measuring device to record the time course activity of the brain. It has been used to monitor brain activity of coma patients, locate areas that has been damaged, and used to predict seizures [7; 22]. Not only is it used to monitor or diagnose the brain but it is used to interact with technology using the brain. Extracted and interpolated commands from EEG can be used to control either a cursor on the screen or an avatar in a virtual environment [3; 30].

2.4 Artifacts

During EEG recording, noise is introduced that contaminates the cerebral electrical activity (EEG) and is known as artifacts [23]. Artifacts are electrical activites that are produced outside the brain (see Figure 2.6) which contaminates and/or obstructs the relevant cerebral activity recorded by EEG. These signals can occur at any point during an EEG recording and amplitudes are usually greater than that of the interested cortical signals [23]. Different types of artifacts can be grouped into physiological artifacts and non-physiological artifacts.

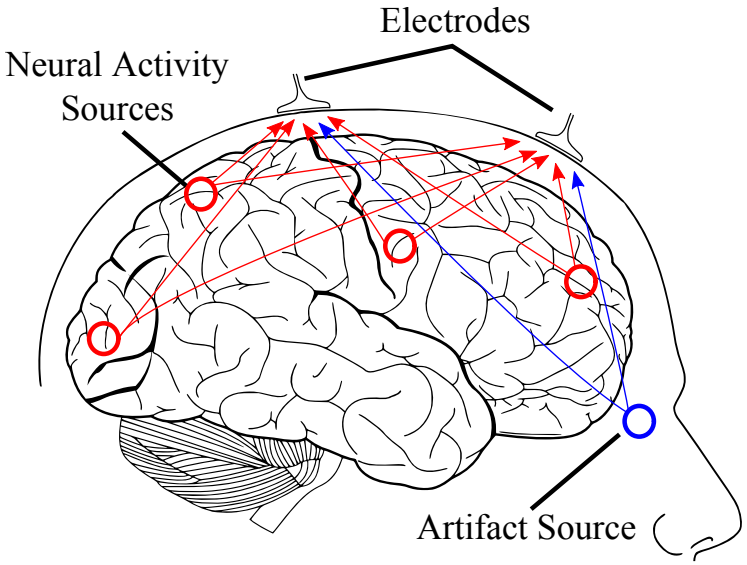

Figure 2.6: Summation of neural activity recorded.

2.4.1 Physiological

Physiological artifacts are generated by the body's activities such as movement and or bioelectrical potentials. Below the most common physiological artifacts found in EEG are briefly explained.

2.4.1.1 Muscle (electromyogram) activity

Muscle artifacts are the most common artifacts in EEG especially during wakefulness. It is produced by frontalis, temporalis, and occipitalis scalp muscles, for example when a subject clenches his jaw, as well as by tongue, neck, and face muscle movements. The electrodes located near or at the scalp muscles (Fp1, Fp2, T7, T8) are mostly affected by the artifact. However, electrodes Cz and Pz are not affected by the arifact because there is almost no muscle over the vertex of the scull [23].

Figure 2.7 shows the EEG activity of electrode T8, located at the midtemporal near the right ear. It is observed that the muscle artifact presents as high frequency waves with spike-like potentials that vary in shape and height. Take note that a bipolar montage was used for the recordings in Figure 2.7.

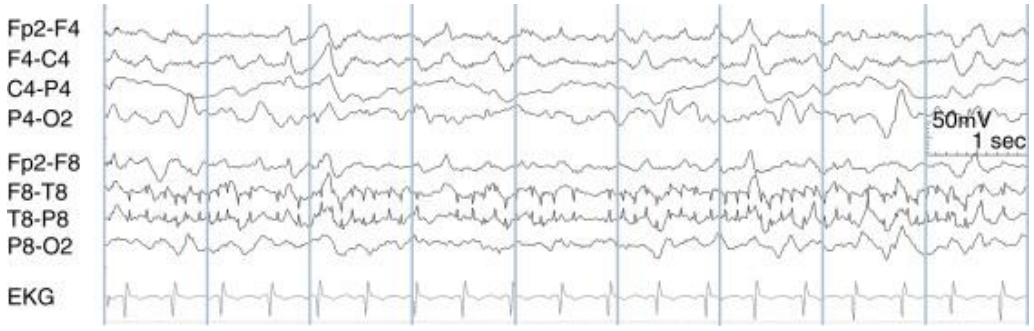

Figure 2.7: Muscle artifacts in EEG [23].

2.4.1.2 Eye Blink

An eye blink artifact is a spike-like wave (see Figure 2.8 channels Fz and Fp2) that is produced by the alteration in conductance during eyelid and cornea contact [31]. The electrical magnitude of an eye blink is around 10 times larger than the original signals and lasts for 200 to 400 ms [31; 32]. Due to such a large magnitude it allows the majority of the signal to propagate throughout the superficial layer while its magnitude decreases rapidly the further it travels from the source. The electrodes located in the frontal region of the scalp is mostly affected by the eye blink artifact. Take note that a bipolar montage was used for the recordings in Figure 2.8.

2.4.1.3 Eye Movement

The eye ball has a positive charge at the cornea (anteriorly) and a negative charge at the retina (posteriorly). During rotation of the eye a large amplitude

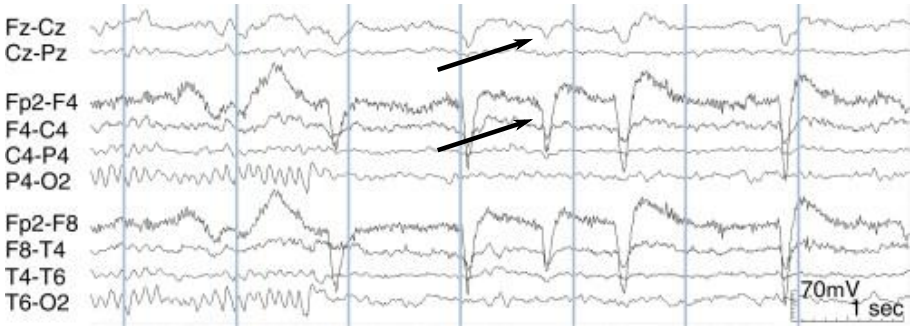

Figure 2.8: Blink artifacts in EEG (adopted from [23]).

alternate current field is generated and is detected by the electrodes located close to the eye, with electrodes F7 and F8 mostly affected [23; 31]. The muscles involved in the movement of the eye produces the rest of the artifacts. Due to the lateral movement of the eye toward F7, a maximum positive charge is induced (see Figure 2.9) where at F8, a maximum negative charge is induced. Take note that a bipolar montage was used for the recordings in Figure 2.9).

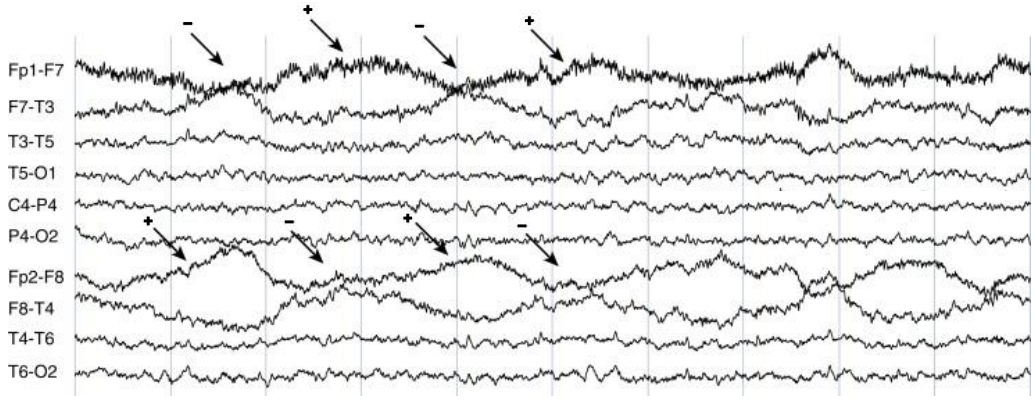

Figure 2.9: Eye movement artifacts in EEG (adapted from [23]).

2.4.1.4 Heart (electrocardiogram) activity

The heart consists of cardiac muscle which receives and distributes an AP that synchronously contracts the heart allowing it to beat. The electrical activity of the heart is conducted to the scalp causing the QRS complex (a series of deflections representing depolarization before contraction) to contaminate the EEG signals. The QRS complex is predominantly observed in the left temporal electrodes because the heart is situated on the left side of the body [23]. It is difficult to distinguish between the QRS complex and desired EEG signals due to the small magnitude it has. Recording the electrocardiogram (EKG) the QRS complex can be identified by comparing the small magnitude spikes

to the timing of the EKG (see Figure 2.10 channel A1-T7). Take note that a bipolar montage was used for the recordings in Figure 2.10).

Figure 2.10: EKG artifacts in EEG (adapted from [23]).

2.4.1.5 Sweat Artifact

Minerals (such as sodium chloride) and lactic acid present on the skin induces a large slow baseline drift (see Figure 2.11 channel F4). This drift is caused by the chemical reaction between the minerals, acid, and metals of the electrode. These minerals that react with the electrode originate from sweat [31; 33].

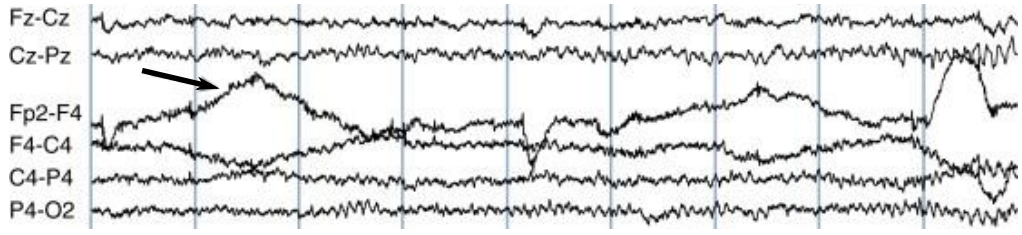

Figure 2.11: Sweat artifacts in EEG [23].

2.4.2 Non-physiological

Non-physiological artifacts are generated by sources outside of the body such as electromagnetic fields generated by power lines or faulty connections between electrodes and skin. Below the most common non-physiological artifacts found in EEG are briefly explained.

2.4.2.1 Power Line

Electrical wiring runs throughout all buildings to deliver power to the desired locations. These power lines produce an electromagnetic signal of 50 Hz (60 Hz) depending on the country's power output and contaminate the EEG signals. The 50 Hz noise has a large electrical amplitude that ranges from 10 mV to 1 V, whereas the desired EEG signals range from 10 to 100 μV (see Figure 2.12 channel P4). It is often necessary to use a notch filter with a null frequency of 50Hz to ensure rejection of the noise [23; 31].

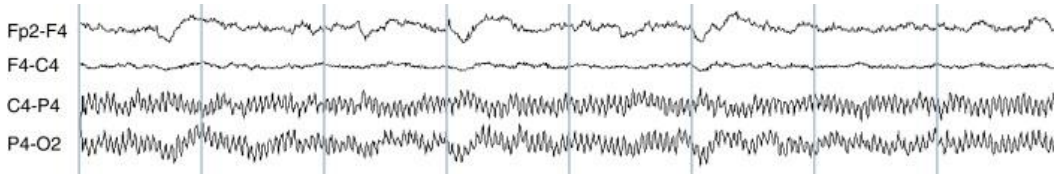

Figure 2.12: Power line artifacts in EEG [23].

2.4.2.2 EEG Electrode

Electrode pop is the most common electrode artifact. During EEG recording there is a buildup of static charge and then a sudden release of that charge. This produces an abrupt vertical transient (see Figure 2.13) which is strictly localized to a single electrode [23]. There are cases where highly repetitive popping occurred in one electrode which resembles seizure activity.

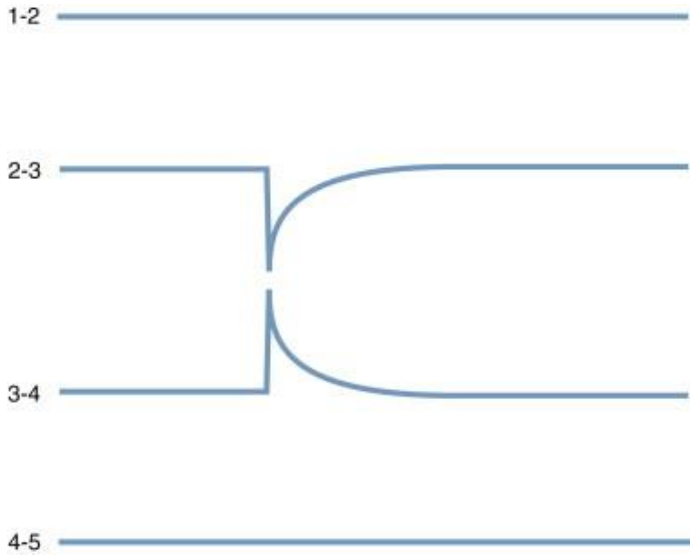

Figure 2.13: Electrode pop artifact shape [23].

2.5 Brain Computer Interface

BCI is a system that provides an alternative communication channel between man and machine. Using neural signals, acquired by EEG, BCI analyses and translates the intention of the individual into commands that a machine can understand and execute. This alternative communication channel allows the brain to bypass the body's motor output pathways and peripheral nerves allowing direct contact. This provides a number of human-machine technological opportunities, such as:

- For Motor impaired subjects;
  - a neural bypass to move a prosthesis [34];
  - a P300 word speller to talk [35]);
  - and a computer cursor control to interact with computers [26]).
- For Healthy subjects;
  - a new method to experience video games and virtual reality [3].

2.5.1 BCI Structure

During the process of recording neural activity to interacting with the machine, a lot of information processing takes place. The BCI structure consists of signal acquisition, pre-processing, signal classification, and machine interaction as seen in Figure 2.14 [19; 26].

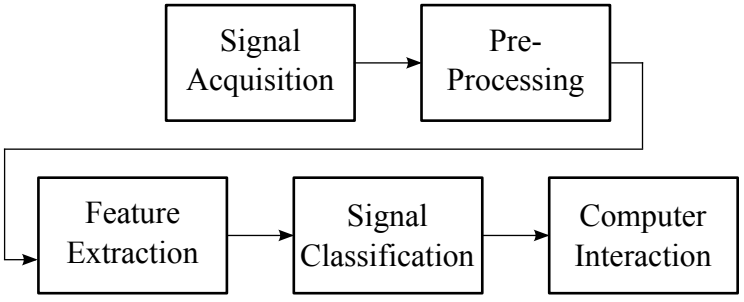

Figure 2.14: Typical structure of BCI [23].

2.5.1.1 Signal Acquisition

During this stage the neural activity of the individual is obtained through invasive or non-invasive methods using electrodes. The recorded neural activity is sampled at a chosen sampling rate and then amplified using amplification equipment.

2.5.1.2 Pre-Processing

The data obtained from signal acquisition is contaminated with artifacts, see Section 2.4, thus it is processed to enhance the signal-to-noise ratio. This ensures that the quality of EEG is of a high standard when classifying the mental tasks. This thesis concentrates solely on this area of BCI to help improve the ease of classification [26].

2.5.1.3 Feature Extraction

After the signal-to-noise ratio has been improved, features such as spatial filtering, voltage amplitude measurement, and spectral analysis are extracted from the data that encode the subjects' message or command. These features can be in the time domain (e.g. evoked potential amplitudes) and/or the frequency domain (e.g. mu or beta-rhythm amplitudes)[24; 1].

2.5.1.4 Signal Classification

Once the features of the EEG are extracted they are classified to determine what mental task the individual is performing. Afterwards, these tasks are converted to device commands that can be understood by today's technology[26].

2.5.1.5 Computer Interaction

Using the mental tasks of the individual, a new set of command algorithms can be developed depending on the use of the BCI[26].

2.5.2 EEG Neural Features used in BCI

Current BCI systems are categorized according to the EEG neural features used. These features can be recorded using both invasive and non-invasive electrodes. The four features that can be recorded using only non-invasive EEG is described below.

2.5.2.1 Visual Evoked Potential (VEP)

VEP is the generation of electrical potentials through visual stimulus using flashing lights. These flashing lights stimulate the visual cortex thus producing electrical potentials that are more prominent in the occipital lobe [36; 37]. This allows the BCI system to determine the direction of the individual's eye gaze. The properties of these generated potentials are depended on the type of visual stimulus used. Steady-state VEP (SSVEP) is produced by a stimulus at a constant frequency which in turn increases the EEG activity at the stimulus frequency [19; 26]. This allows BCI to determine the individual's choice on a screen by flashing each choice at a different frequency then comparing it to the EEG frequency peaks.

2.5.2.2 Slow Cortical Potential (SCP)

SCPs are slow changes in the brain's electrical potentials and is produced by either excitation (increase in SCP) or decrease in excitation (decrease in SCP) of the cortex. These changes normally occur in low frequency bands (less than 2 Hz) and last from 500 ms to several seconds [37]. Individuals can be trained with visual feedback to control these changes that are used in BCI as a means of controlling a cursor's movement, but SCP is not restricted to only cursor movement.

2.5.2.3 P300 Evoked Potential

Infrequent and particular stimuli used to evoke a positive peak is known as P300 evoked potential. Auditory, visual, or somatosensory stimulation is used that produces a positive peak at about 300 ms after the simulation. The phenomenon is predominately located over the central parietal region [19]. The first use of P300s in BCI has been demonstrated by [35] where in a 6x6 matrix, containing all 26 letters of the alphabet and 10 digits, rows and columns were randomly highlighted while the individual concentrated on a single letter. The correct letter was determined by finding the row and column pair that produced the P300.

2.5.2.4 Event-Related De/Synchronization (ERD/ERS)

Mu (8-13Hz) and beta (13-30 Hz) rhythms originate from the motor and sensorimotor cortex located between the frontal and parietal lobe. These signals are present when an individual is stationary. However, during a voluntary or imaginary motor movement, the signals are suppressed/desynchronized and a decrease in power is observed which is known as ERD. After the movement is completed the suppression/desynchronizing of mu and beta rhythms are decreased thus increasing the power. The increase in power is known as ERS. ERD occurs 0.5-2 s before the movement and starts at the contralateral rolandic region but becomes bilaterally symmetrical immediately prior to movement [36; 38]. ERS occurs at about 600 ms after movement is complete and occurs predominately over contralateral sensorimotor area [36]. Mackay [38] observed that the average frequency of the ERS that takes place for beta rhythms are different for each set of motor movement.

Chapter 3

Signal Processing Methods

In order to remove eye blink artifacts, the EEG content must be analysed in the frequency domain to temporally locate the artifact. The artifact must be removed without distorting any neural activity. To accomplish this, a combination of ICA, wavelet analysis, and neural networks has been proposed. ICA, using blind source separation, separates EEG into separate independent source components, one of which would be the eye blink artifact, without distorting the EEG. Wavelet analysis transforms the EEG data into time-frequency representations which is used to detect and correct eye blinks. The eye blink artifacts will also be corrected using a trained neural network. This chapter describes the theoretical background for ICA, wavelet analysis, and neural networks.

3.1 Independent Component Analysis

ICA is a special case of blind source separation (BSS) which recovers linear independent mixed sources, using higher order statistics, to separate multivariate signals by reducing their statistical dependence. ICA has been used in blind source separation and feature extraction with emphasis on EEG [9; 39; 40].

3.1.1 Cocktail Party

The cocktail party problem is the most commonly used and rudimentary example used to explain the concept of ICA. Figure 3.1 shows that there are three individuals in a room speaking simultaneously while three microphones at different position within the room record their conversations simultaneously. Each recording will thus be a mixture of all the conversations where recordings are dependent on the distance and volume of each individual. Applying ICA to the three recordings allows each individual's conversation to be separated without the interference of the other two.

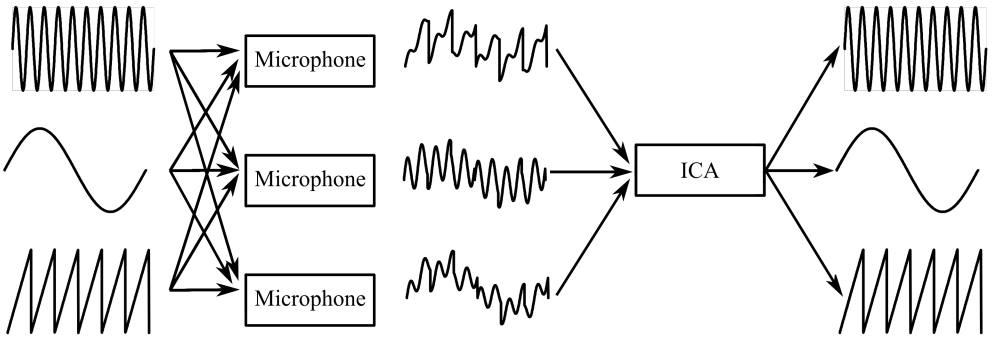

Figure 3.1: Illustration of ICA applied to cocktail party problem.

3.1.2 Theoretical Background

The simplistic BSS mixing model, which makes no assumptions, represents a realistic model for a system where the observed vector $\mathbf{k}(t) = [k_1(t), k_2(t), \ldots, k_m(t)]^{\mathbf{T}}$ is determined by a source vector $\mathbf{s}(t) = [s_1(t), s_2(t), \ldots, s_n(t)]^{\mathbf{T}}$ and additive sensor noise $\mathbf{n}(t)$ where the source vector is mixed by an unknown mixing function, $\mathbf{f}$ as seen in 3.1.1 [41].

$$\mathbf{k}(t) = \mathbf{f}\mathbf{s}(t) + \mathbf{n}(t) \tag{3.1.1}$$

In order to determine the sources, information is required of $\mathbf{f}$, $\mathbf{n}$, and $\mathbf{k}(t)$ which makes the BSS model intractable. However when formulating ICA, assumptions are made about the signals to simplify the problem making it more tractable. Firstly, it is assumed that there is no noise present in the system. This makes the model more unrealistic because during source separation the sources can be contaminated with noise. Secondly, the mixing of the sources is assumed to be linear and the transmission through mixing medium is instantaneous (instantaneous mixing). Thirdly, the number of sources is assumed to be equal to the number of observed signals ($m = n$). Fourthly, the sources are statically independent meaning independent variables have no higher order correlation and are uncorrelated [41]. Lastly, the sources of the observed signals are assumed to be stationary. These assumptions reduces 3.1.1 to,

$$\mathbf{k}(t) = \mathbf{A}\mathbf{s}(t) \tag{3.1.2}$$

where $\mathbf{A}$ is the square linear mixing matrix [40; 41; 42; 43]. In order to determine the sources from 3.1.2, ICA determines the unmixing matrix $\mathbf{W}$, the inverse of $\mathbf{A}$, and determines the sources using 3.1.3 [41; 43; 44].

$$\mathbf{s}(t) = \mathbf{W}\mathbf{k}(t) \tag{3.1.3}$$

The sources determined by 3.1.3 are not the true sources of the observed signals because an assumption was made that there is no noise present in the

system, thus the noise present is mixed with the true sources.

There exist many different ICA tools, each applicable under some specific assumption (for the static model of the sources) such as non-Gaussian (NG), non-stationary (NS), spectral density (SD), and hybrid (combination of assumptions) [45]. For the purpose of this thesis the assumption of NG was used and will now be discussed [41; 46]. Furthermore from [47] it was determined that INFOMAX, which is a form of ICA analysis that uses negentropy to measure independence, produces the best results producing independent source components and thus it will be used throughout this thesis.

3.1.3 Independence with Non-Gaussian

Independence is defined by the probability density function (pdf) and states that any one independent source component must not contain any information regarding other independent source components. If the joint pdf is symmetric (Gaussian) then source estimation becomes impossible with ICA and thus a system with more than one Gaussian independent source component will not work with this analysis [45]. However, due to the central limit theorem, the mixture of non-Gaussian random variables results in a distribution closer to Gaussian than their original variables. The sources can be assumed to be non-Gaussian even if the mixture of sources appears Gaussian [45]. Thus non-Gaussianity can be used as a measure to determine independent source components.

In order to determine one independent source component, consider a linear combination of k_m, see 3.1.3, where $\mathbf{w}$ is a unmixing vector that must be determined. Therefore by replacing the coefficient $\mathbf{w^T A}$ with $\mathbf{z}$ produces a source signal function, see 3.1.4 [42].

$$y = \mathbf{w}^T\mathbf{k} = \mathbf{w}^T\mathbf{A}\mathbf{s} = \mathbf{z}^T\mathbf{s} \tag{3.1.4}$$

Due to the central limit theorem, $\mathbf{z}^T\mathbf{s}$ is more Gaussian than any of the sources s_m. Thus, by assuming s_m to have identical distribution, only one element of z_m is non zero. Therefore maximizing the non-Gaussianity by varying w will result in y_m being an independent source component. In order to find all independent source components all local maxima needs to be determined [42].

There exist statistical methods that can be used to quantify the non-Gaussianity of random variables, such as kurtosis and negentropy. INFOMAX uses negentropy, which is based on the information-theoretic quantity of differential entropy, to quantify and maximize non-Gaussianity. Entropy, a basic concept of information theory, is the measure of disorder [42]. For example, the more unpredictable a random variable is, the greater the entropy. For a discrete

random variable Y, entropy H is defined as

$$H(Y) = -\sum_i P(Y = a_i) log P(Y = a_i) \tag{3.1.5}$$

where a_i represent the possible values of Y and P represent the probability [42]. For continuous-valued random variables differential entropy H is defined as

$$H(\mathbf{y}) = -\int f(\mathbf{y}) log f(\mathbf{y}) d\mathbf{y} \tag{3.1.6}$$

where $\mathbf{y}$ represents a random variable and $f(\mathbf{y})$ represents the density of the random variable [42]. Entropy can be used to measure non-Gaussianity because Gaussian random variables has the largest entropy among all random variables with equal variance which is a fundamental result of information theory [42]. In order to obtain a zero non-negative non-Gaussianity for Gaussian variables, a slightly modified version of differential entropy is used. The modified version is known as negentropy J and is defined as

$$J(\mathbf{y}) = H(\mathbf{y}_{gauss}) - H(\mathbf{y}) \tag{3.1.7}$$

where $\mathbf{y}_{gauss}$ represents a Gaussian random variable of the same covariance matrix as $\mathbf{y}$ [42]. Negentropy is always a non-negative due to the large entropy of Gaussian random variables but is zero for Gaussian random variables. Even though using entropy as a measure for non-Gaussianity is justified by statistical theory, it is computationally very difficult [42].

3.1.4 Preprocessing

Before ICA is applied some pre-processing is done in order to simplify the data, thus allowing the ICA algorithm to perform faster with greater robustness.

3.1.4.1 Centering

Removing the sample mean from the observation vectors is the most basic and necessary pre-processing step since it simplifies ICA estimation. The process of making $\mathbf{k}$ a zero-mean variable does not affect the mixing matrix, thus after the source signals are determined, the mean can be added to each independent source component. This is done by $\mathbf{Wm}$ or $\mathbf{A^{-1}m}$ where $\mathbf{m}$ is the mean subtracted [42].

3.1.4.2 Whitening

The next useful step in pre-processing the data before ICA is applied is known as whitening. Whitening is a process by which the observed vector $\mathbf{k}$ is transformed linearly thus obtaining a new vector $\widetilde{\mathbf{k}}$ whose elements are uncorrelated

with equal unit variance [42]. Thus the transformed data has a covariance matrix equal to the identity matrix. Eigen-value decomposition is a popular method used for whitening. Eigen-value decomposition is applied to the covariance matrix 3.1.8 [42], where $\mathbf{\Lambda}$ is the orthogonal matrix of eigenvectors, $\mathbf{D}$ is the diagonal matrix of eigenvalues, and $\mathbf{E}$ is the orthogonal matrix of $E\{\widetilde{\mathbf{k}}\widetilde{\mathbf{k}}^{\mathbf{T}}\}$. Using 3.1.9 [42] the data is whitened and the original vector is transformed as indicated by 3.1.10 [42].

$$E\{\widetilde{\mathbf{k}}\widetilde{\mathbf{k}}^{\mathbf{T}}\} = \mathbf{\Lambda}\mathbf{D}\mathbf{E}^{T} \tag{3.1.8}$$

$$\widetilde{\mathbf{k}} = \mathbf{\Lambda}\mathbf{D}^{-1/2}\mathbf{\Lambda}^{T}\mathbf{k} \tag{3.1.9}$$

$$\widetilde{\mathbf{k}} = \mathbf{\Lambda}\mathbf{D}^{-1/2}\mathbf{\Lambda}^{T}\mathbf{A}\mathbf{s} = \widetilde{\mathbf{A}}\mathbf{s} \tag{3.1.10}$$

Whitening reduces the complexity of estimating the mixing matrix thus improving the performance of ICA. This is accomplished by reducing the number of parameters to be estimated from n^2 ($\mathbf{A}$) to $n(n-1)/2$ ($\widetilde{\mathbf{A}}$) [42].

3.1.5 ICA for source separation of EEG activity

Areas in the brain such as the motor cortex, occipital lobe etc. are spatially fixed sources that generate neural activities independent from one another. EEG data recorded at multiple sensors are a linear mixture of these sources where mixing and propagation throughout the brain towards the sensors are instantaneous. Eye blink neural activity is independent from that of the brain's neural activity because it is a completely different generating mechanism not related to the cortex activity [31; 42]. ICA applied to the EEG data allows the different sources to be separated. This allows artifacts to be separated into their own independent sources and removed from the EEG data. However, these sources are but estimates of the true sources, thus artifact sources can still contain some other neural activity source. Examples of studies that has applied ICA are discussed in [9; 40; 45].

3.2 Wavelet Analysis

Wavelet analysis is a technique that uses wavelet functions to simultaneously measure time and frequency variation of a signal. The wavelet transform has many advantages for signal processing due to its ability to optimize a wavelet function for a non-stationary signal [48]. Thus the function's properties can be used in a variety of signal processing applications.

3.2.1 Theoretical Background

In order to classify an oscillating amplitude scaling function as a wavelet it must first satisfy several requirements. The wavelet ψ must have zero mean

amplitude with finite energy over its time course and relatively larger higher frequency energy compared to its lower frequency energy [49]. Therefore a sine wave which extend infinitely in time and has infinite energy cannot be classified as a wavelet even though it has zero mean amplitude. Wavelets are able to be localized in time and frequency because, not only being band-limited in their frequency domain, their amplitudes have large fluctuations within a constrained time period and miniscule amplitudes outside of the time period [49].

The wavelet chosen to transform a signal into a representation that demonstrates frequency content at different points in time is known as a mother wavelet. The mother wavelet, which can be scaled, dilated, stretched, compressed and translated without changing their basic shape, contributes to a wavelet family which consists of many mother wavelets [2; 49]. The scaling variable s and translation variable u are the basic parameters of wavelet representation shown by (3.2.1) [49; 50; 15]. These variables are used to adjust the size (s) and transfer (u) the mother wavelet in time in order to match a part of the processed signal.

$$\psi_{u,s}(t) = \frac{1}{\sqrt{s}}\psi\left(\frac{t-u}{s}\right) \tag{3.2.1}$$

Stretching allows the wavelet to become less localized in the time domain (more spread out) and more localized in the frequency domain while shrinking makes it more localized in the time domain and less localized in the frequency domain. As a result wavelets obey the Heisenberg uncertainty principle stating that time localization trades off against frequency localization as wavelets are scaled [49].

Traditional techniques like the short time fourier tranform (STFT) consist of a series of fourier transforms with a fixed window size that has the capability to represent the waveform in the time and frequency domain. Due to the fixed window size, STFT can only have an optimal resolution for a single point in time or space since each point in time or space requires a unique window [49]. Thus, the fixed window size produces suboptimal resolution at other points in time or space. Wavelets alternatively has the ability to adjust their window size which allows it to reach an optimal size for the entire range thus having a considerable advantage over STFT [49].

The continuous wavelet transform (CWT) computes wavelet coefficients by manipulating (scaling and translating) the basic shape of the wavelet in infinite small steps in relation to a continuous signal. Using (3.2.2 [50]) infinite wavelet coefficients, $c_{s,u}$, of a continuous signal, $f(t)$, can be determined by infinitely adjusting s and u where $*$ indicates the complex conjugate. In or-

der to realistically implement CWT the wavelet must meet the admissibility condition (see 3.2.3 [50]) which in turn makes the inverse transform and Parseval's theorem applicable [50]. This allows a usefull reconstruction of the deconstruction of a continuous signal.

$$F(u,s) = \int_{-\infty}^{\infty} f(t)\frac{1}{\sqrt{s}}\psi^*\left(\frac{t-u}{s}\right)dt \tag{3.2.2}$$

$$\int_{-\infty}^{\infty} \psi(t)dt = 0 \tag{3.2.3}$$

Mallat [2; 49] developed the discrete wavelet transform (DWT) to compensate for the inefficiency of CWT caused by the redundancy that occurs when displaying closely spaced time points. DWT efficiency arises from the fact that it produces a finite number of coefficients (same number as signal samples) without loss of any information where CWT produces an infinite amount [49]. This allows for perfect reconstruction of the signal if all coefficients are known.

DWT produces wavelet coefficients by passing the original signal (n samples) through low and high pass digital filters where the filters' impulse response is determined by the particular wavelet chosen for analysis. Each filter produces a series of wavelet coefficients, which is the same length as the original signal. Afterwards these coefficients are downsampled by two, producing approximate (n/2 samples) and detailed coefficients (n/2 samples) [49] as seen in Figure 3.2(a). The output of the high pass filter is the set of wavelet coefficients and the output of the low pass filter is a set of scaling function coefficients which represents a relationship between the source signal and the wavelet chosen. The original signal or any level of decomposition can be reconstructed (see Figure 3.2(b)) because all the coefficients are preserved [49]. The reconstruction process is the mirror image of the decomposition process where the coefficients are interpolated, filtered and summed.

The original signal can be decomposed more than one level to produce much smaller frequency bands. In order to decompose the signals to a lower level the approximate coefficients are used as the signal and the decomposition process is repeated, while the detailed coefficients are stored. This produces two new sets of coefficients; each one-fourth the original size of the signal. This process is repeated until the desired level of decomposition is achieved [49]. Figure 3.3 shows an example of how the frequency bands are arranged. In this figure, f_0 is the centre frequency and Δf is the bandwidth of the detailed coefficients of a fourth level decomposition. The detailed coefficients' bandwidth are half of the previous band for each level of decomposition, thus providing an improvement in frequency resolution with each successive larger detail band. This shows that a constant scale of the wavelet filter ($\frac{f_0}{\Delta f}$) is held by wavelets used as octave harmonic filters, which is known as the constant Q property.

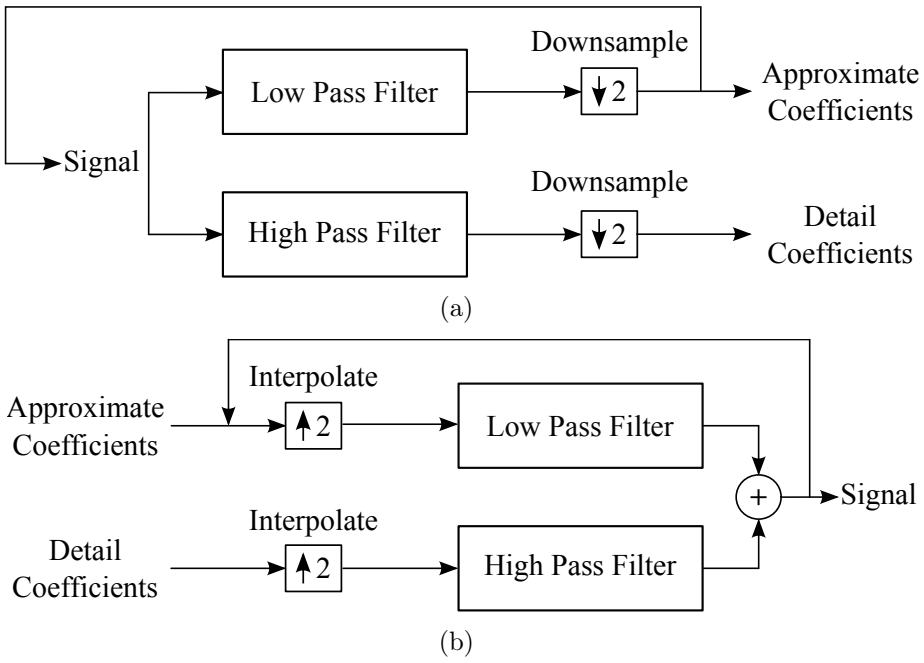

Figure 3.2: Basic filter process of DWT for a) decomposition and b) reconstruction (adapted from [49]).

EEG frequency bands delta, theta, alpha, beta, and gamma closely resemble the constant Q pattern, thus making wavelet analysis ideal for associating frequency bands with eye blinks [49].

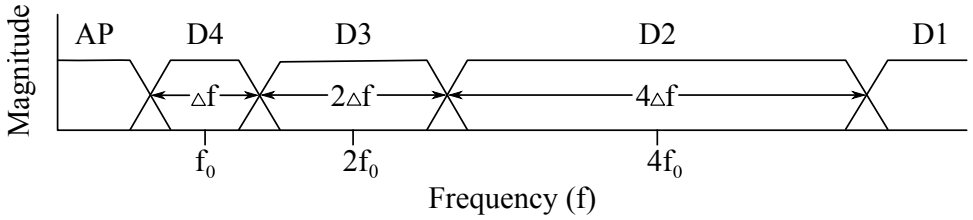

Figure 3.3: Illustration of frequency bands arrangement after decomposition (adapted from [49]).

3.2.2 Wavelet Analysis for Detecting Patterns in EEG

Patterns present in EEG signals have a high frequency and low amplitude with small time periods. Applying wavelet analysis is advantageous due to the fact that the smaller the duration of the neural event, the greater the time resolution of the wavelets will be, thus patterns with a miniscule duration can also be detected with great accuracy. [49]. Even if the event overlaps with

another in time, accurate event detection is still accomplished due to precise control of frequency selectivity introduced by the wavelet packets. This allows artifacts to be specifically targeted for detection and extraction. Examples of studies that have applied wavelet transform are discussed in [51; 39; 52].

3.3 Artificial Neural Networks

The human brain is a vast neural network that consists of interconnecting nerve cells (neurons) which transfers and processes information in the form of electrical signals. The neural network of the brain is capable of remarkable information processing such as high parallelism, nonlinearity, robustness, ability to handle fuzzy and precise information, and the capability to generalize [53]. McCulloch and Pitts [54] were the first to duplicate these information processing characteristics by developing an artificial neural network (ANN). ANNs are simple processing units or computational models that replicates the brain's method of acquiring knowledge from the environment through learning and storing the acquired knowledge using synaptic weights [53]. This chapter discusses the basics of neural networks as well as the neural network and training method used in this thesis.

3.3.1 Perceptrons

Like the neural network of the brain consists of neurons, the ANN consists of perceptrons. The perceptron, see Figure 3.4, consists of input connections (dendrite of axon), an activation function (cell body), and an output connection (axon)[53].

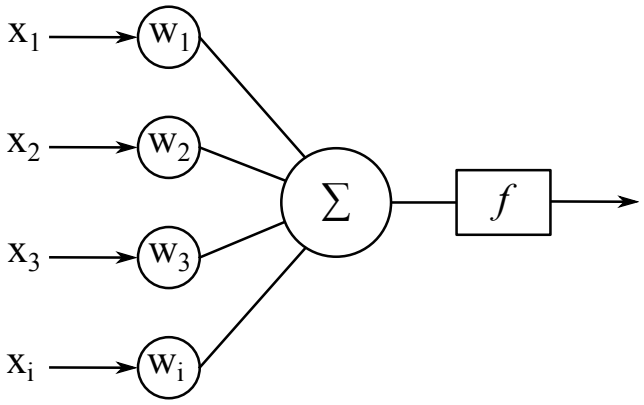

Figure 3.4: Illustration of a perceptron.

Perceptrons function in the exact same manner as neurons where it receives a

stimulus, and if it passes the threshold, it transmits a signal to another perceptron. The output g can be mathematically expressed as

$$g = f\left(\sum_{i=1}^{N} \omega_i x_i - \omega_{TH}\right) = f\left(\sum_{i=0}^{N} \omega_i x_i\right) = f(z) \tag{3.3.1}$$

where x_i represents one of the inputs, ω_i represents the input's associated weights, ω_0 represents the threshold value, and f represents a monotone threshold function [53; 24]. Monotone threshold functions represent the AP that is produced by the stimulus surpassing the threshold. For example a monotone function such as the Heaviside function $L(z)$, see equation 3.3.2 [24], produces a zero value if inputs are negative (inhibitory reaction) and a unity value if inputs are positive (excitatory reaction).

$$L(z) = \begin{cases} 1 & z \geq 0 \\ 0 & z < 0 \end{cases} \tag{3.3.2}$$

Many perceptrons linked together, like neurons in the brain, form an artificial neural network. Figure 3.5 illustrates a single layer neural network which consists of an input layer, a hidden layer, and an output layer. The input layer receives information from the environment and the hidden and output layer consists of weights processing the information [24]. During training the network is guided by providing the desired output for all presented input. This allows the network to compare its output to the desired output and adjust the weights of the hidden and output layer accordingly [24]. This method of training is known as supervised learning.

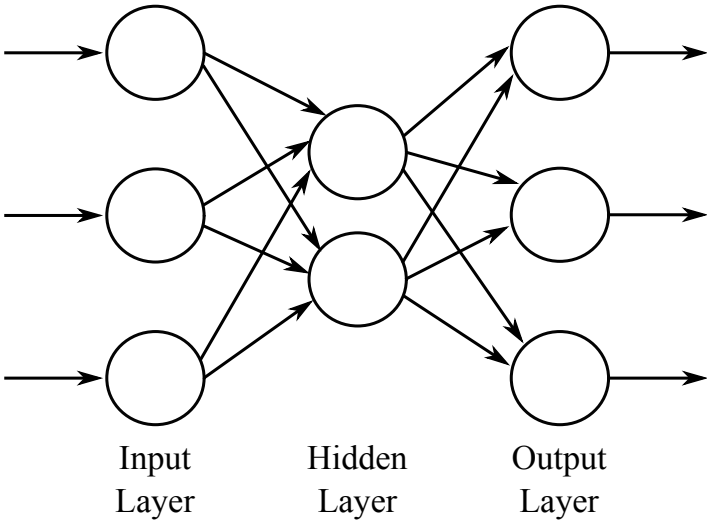

Figure 3.5: Structure of a single layer artificial neural network.

3.3.2 Multilayer Network

The ANN in Figure 3.5 is limited because it cannot solve a classification problem if the classes are not linearly separable. To overcome this problem the multilayer ANN was introduced. Figure 3.6 illustrates a 3 layer network where there are 2 hidden layers and 1 output layer. Note the input layer is not included because it does not take part in the training of the network but only distributes the inputs to the hidden layers [24].

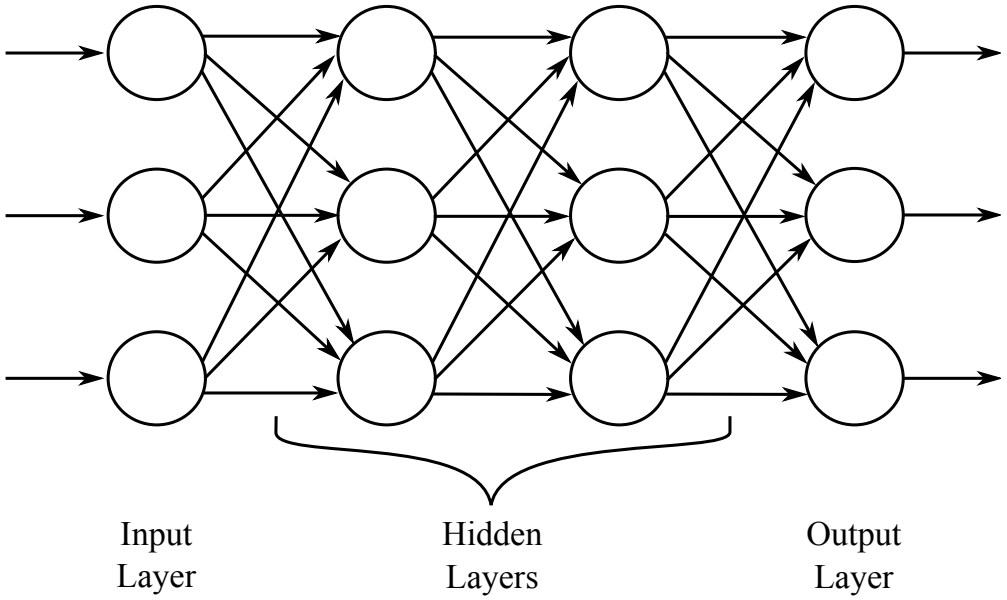

Figure 3.6: Structure of a 3 layer artificial neural network.

The multilayer ANN is classified based on its characteristics such as learning algorithm, direction of information flow, the function of the ANN etc. The feedforward backpropagation ANN, used in this thesis, is a multilayer network that has no feedback from the output to the input layer and has been trained using the backpropagation learning algorithm. The advantage of this network is its ability to represent non-linear functions [24].

3.3.3 Resilient Backpropagation Training

The backpropagation, a supervised training algorithm, is the most widely used method of training ANNs. It makes use of the gradient decent principle to search for a minimum error on an error surface and changes the weights accordingly. During each iteration two sweeps occur: a forward activation sweep to produce an output which is compared to the target output, and a backwards sweep where the error between the output and target is used to adjust the weights from the output layer, through all the hidden layers, to the input

layer [53]. The goal is to minimize the global error E defined as

$$E = \frac{1}{R}\sum_{R=1}^{R} E_R \tag{3.3.3}$$

where R represents the total number of training patterns and E_R represents the training pattern r error [55]. E_R is determined by

$$E_R = \frac{1}{2}\sum_{i=1}^{N}(G_i - X_i)^2 \tag{3.3.4}$$

where N represents the total number of output nodes, G_i represents the network output, and X_i represents the target output at the i^{th} node [55]. The aim of minimizing the error function E is achieved by determining the partial derivative of each weight, and then performing the simple gradient descent defined as

$$\omega_{ij}(t+1) = \omega_{ij}(t) - \varepsilon\frac{\partial E}{\partial \omega_{ij}}(t) \tag{3.3.5}$$

where ω_{ij} represents the weight from neuron j to neuron i, $\frac{\partial E}{\partial \omega_{ij}}$ represents the partial derivative of the weight, and ε represents the learning rate which scales the derivative [53; 56]. Thus the next weight with the smallest error compared to the previous weight's error can be determined. However, during the search for the minimum, the algorithm can get caught in a local minimum thinking it is the best solution where there is still a global minimum.

Resilient backpropagation is an efficient learning algorithm that is an improvement on the standard backpropagation algorithm. Instead of weights updating after each iteration, like backpropagation, the resilient backpropagation updates the weights after each pattern, speeding up the process of finding the global minimum. This is achieved by an individual update-value $\triangle_{ij}$ for each weight, which only determines the size of the weight update. Using equation 3.3.6 [56] the update-value changes during the learning process based on the error function E.

$$\triangle_{ij}(t) = \begin{cases} \eta^+ * \triangle_{ij}(t-1), & \text{if} \frac{\partial E}{\partial \omega_{ij}}(t-1) * \frac{\partial E}{\partial \omega_{ij}}(t) > 0 \\ \eta^- * \triangle_{ij}(t-1), & \text{if} \frac{\partial E}{\partial \omega_{ij}}(t-1) * \frac{\partial E}{\partial \omega_{ij}}(t) < 0 \\ \triangle_{ij}(t-1), & \text{else} \end{cases} \tag{3.3.6}$$
$$\text{where } 0 < \eta^{-1} < 1 < \eta^+$$

The above equation states that every time the partial derivative, of the corresponding weight ω_{ij}, changes its sign, the update-value $\triangle_{ij}$ is decreased by a factor η^- which indicates that the algorithm's previous update was too big and missed the local minima. When the partial derivative sign stays constant, the

update-value is increased by a small amount which accelerates the convergence [56].

The weight-update follows its own rule, see 3.3.7 [56], after the update-value of each weight is updated. It states that if the partial derivative is positive, the weight is decreased by its update-value and when it is negative, the weight is increased by the update-value [56].

$$\triangle\omega_{ij}(t) = \begin{cases} -\triangle_{ij}(t), & \text{if} \frac{\partial E}{\partial \omega_{ij}}(t) > 0 \\ +\triangle_{ij}(t), & \text{if} \frac{\partial E}{\partial \omega_{ij}}(t) < 0 \\ 0, & \text{else} \end{cases} \tag{3.3.7}$$
$$\text{where } \omega_{ij}(t+1) = \omega_{ij}(t) + \triangle\omega_{ij}(t)$$

After the entire pattern set is introduced once to the network, the update-values and weights are changed. This change starts from the output layer, and works its way through the hidden layers until it reaches the input layer.

3.3.4 ANN for detecting and correcting patterns in EEG

Each individual is unique and so are the EEG wave patterns generated by each individual's brain. This makes it difficult to design a method that detect certain EEG patterns and be used on any individual. ANN mimics the brain's processing properties (see Section 3.3) thus, ANN has a lot of potential regarding EEG information processing. For example if an ANN is trained to detect an EEG pattern, even if the repeated pattern does not match the training pattern, the ANN will still detect it due to its ability to generalize. Examples of studies that has applied ANN are discussed in [26; 57; 15].

Chapter 4

EEG Signal Simulation

Different methods and algorithms have been designed to separate or remove the artifacts from the neural activity with good results, but it is unclear quantitatively how well the artifact is removed while the neural activity remains the same. In order to determine how well the artifact is removed from the neural activity without distorting it, an artifact free EEG signal and artifact containing EEG signal (derived from the artifact free signal) is required. De Beer et al. [16] introduced a method where a single EEG signal can be generated and impregnated with different types of artifacts. This provides a means to compare the original artifact free EEG data to the resulting EEG data of the algorithm and determine its performance. This chapter briefly discusses the model and filter design used by [16] to generate a single EEG signal. Afterwards, the artifact signal generation is discussed in detail.

4.1 Signal Generator Model

There exist two possible methods for generation of the basic EEG signal. One such method is simulating each individual neuron of the brain, which will provide a better understanding of the brain, however this method will be time and power consuming. Another method is to simply simulate the resulting EEG signal of the brain by using a mathematical, electrical, or mechanical model. It allows external effects of multiple variables, such as blood pressure and oxygen saturation, to be considered simultaneously [16].

De Beer et al. [16] designed a signal generator that simulates the EEG activity of a single signal which is based on three assumptions. Firstly, small segments of spontaneous EEG can be described using linearly filtered, normally distributed noise. Secondly, the filtering characteristics can be changed to simulate non-stationary parts in the spontaneous EEG and lastly, if the spectrum of the applied filter resembles that of actual EEG then the signal resulting from the filter process will resemble an actual EEG.

As seen in Figure 4.1 the simulation model consists of a Gaussian white noise generator, filters, gains, and transients. The noise is filtered into five frequency bands, corresponding to the conventional EEG frequency bands (see Table 4.1). Each frequency band is passed through its own gain, see Table 4.1, which allows independent control of their power and amplitude. Afterwards all the frequency bands are summed and passed through a final gain. Transients, a brief abnormal change in EEG, or artifacts can be added to the simulated signal during the summing phase. Even though the simulation is limited to a maximum frequency range of 30 Hz it is sufficient for quantitative analysis and training.

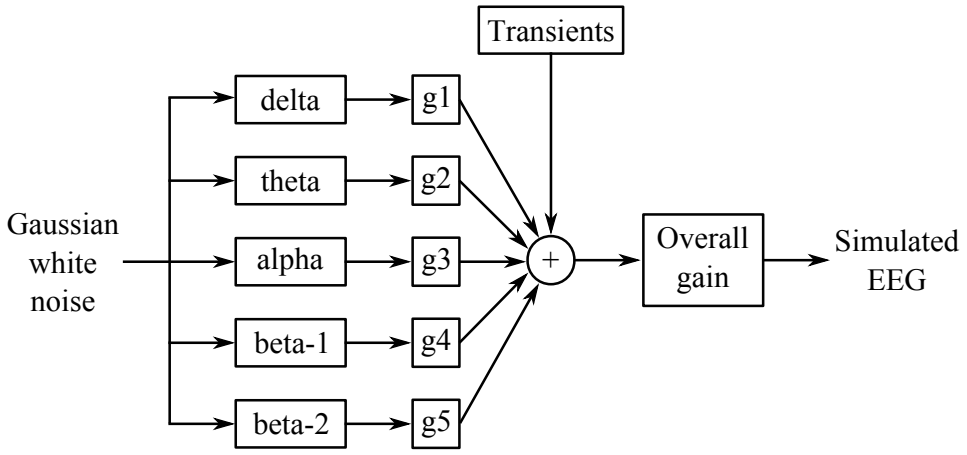

Figure 4.1: Illustration of the EEG simulation model [16].

Table 4.1: Frequency bands name, range and gain (adapted from [16]).

	Lower frequency border (Hz)	**Upper frequency border (Hz)**	**Gain (μV)**
delta	0	4	50
theta	4	8	25
alpha	8	13	25
beta-1	13	20	15
beta-2	20	30	10

4.2 Filter Design for Model

Based on the model, decisions were made by [16] that simplifies the design process. Firstly, the shape of the filters were fixed which reduces the number of

Table 4.2: Parameterized frequency bands [16].

	Bandwidth (Hz)	**Center frequency (Hz)**
delta	2.1	2.0
theta	1.9	5.3
alpha	2.1	10.2
beta-1	4.0	14.0
beta-2	4.3	23.6

variables leaving only the gains which is sufficient for simulating EEG characteristics. Lastly, the frequency bands were parameterized (see Table 4.2) into a center frequency and bandwidth (range between -3dB points) which satisfied the requirement that the parameters should reflect the essential elements of EEG spectral peaks. The side lobes' maximum amplitude was limited to 10% of the main lobe amplitude to reduce the overlapping of lobes that occur.

De Beer et al. [16] made use of a bandpass finite impulse response (FIR) filter and a window, of appropriate length, to produce a frequency transfer function that reproduces the shape of EEG peaks. After analysing different windowed methods, a Hann window produced the best results and met the requirements for the side lobes limitation. The final filter coefficients $q(n)$ and frequency spectrum $Q(e^{j\omega})$ after applying the Hann window is

$$h(n) = (0.5 - 0.5\cos(2\pi\frac{n-\frac{U}{2}}{U}))\frac{\sin b\pi n - \sin a\pi n}{\pi n} \text{ for } -\frac{U}{2} \leq n \leq \frac{U}{2} \quad (4.2.1)$$

$$H(e^{j\omega}) = (b-a) + \sum_{n=1}^{\frac{U}{2}} \left(1 - \cos(2\pi\frac{n-\frac{U}{2}}{U})\right)\frac{\sin b\pi n - \sin a\pi n}{\pi n}\cos \pi n \quad (4.2.2)$$

where $a\pi$ represents the lower cut-off frequencies, $b\pi$ represents the higher cut-off frequencies, and U represents the order of the FIR filter [16]. The filter parameters a, b, U are shown in Table 4.3 which was determined using a sampling frequency of 256 Hz.

Table 4.3: Estimates for filter parameters a,b, and U (adapted from [16]).

	a	**b**	**U**
delta	0.0155	0.0157	240
theta	0.0413	0.0415	260
alpha	0.0796	0.0798	240
beta-1	0.109	0.110	124
beta-2	0.184	0.185	140

4.3 Artifact Signal Generation

Following the process in Figure 4.2, recorded EEG data containing the desired artifact, see Section 5.1.1, is broken into independent source components using ICA. The independent source component containing the artifact is passed through a low pass FIR filter (cut off frequency at 4 Hz) to remove any underlying activity present in the independent source component. Through visual inspection each artifact was enclosed in a small window thus reducing the amount of low frequency data that is still present with the artifacts. Afterwards, these windows containing artifacts and a small amount of low frequency data are removed from the independent source component and interpolated due to the difference in sampling rate between the simulated EEG signal (256 Hz sampling rate) and the Emotiv epoc (128 Hz sampling rate). The interpolated windows of artifact data is used to impregnate the artifact free EEG signal, which was generated by the EEG simulation model, to produce an artifact containing EEG signal.

Due to the nature of the training process for neural networks, the low frequency data extracted with the artifacts will be recognised as part of the artifact and thus will also be corrected. Therefor, the authenticity of the artifact containing EEG signal is dependent on the accuracy of the artifact extraction process.

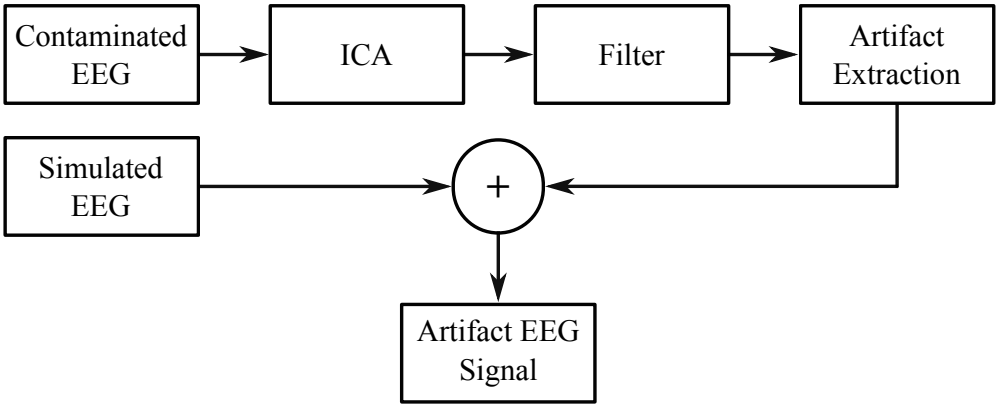

Figure 4.2: Flow diagram of artifact EEG simulation.

Chapter 5

Experimentation and Implementation

In this chapter the experimental setup and data acquisition is discussed as well as the overall process of the algorithms, the evaluation methods, and the testing procedure.

5.1 EEG Data

In order to test the blink detection, blink correction, and overall process, different datasets were required. In the section, each dataset experimental setup and data acquisition is discussed as well as its purpose.

5.1.1 Blink Data

The blink EEG data was recorded at the Biomedical Engineering Research Group lab (University of Stellenbosch) using a 14 channel Emotiv epoc (Emotiv, San Francisco, USA) system at a sampling rate of 128 Hz. The data was collected from two healthy subjects, one male (24 years of age) and one female (23 years of age). During the experiment each subject was seated comfortably and asked to blink normally for 40 s while staring at a fixed point displayed on a screen. Each blink was marked manually as the experiment took place. The male subject completed 10 trials and the female subject completed 15 trials. The experiment produced 25 trials in total, each trial lasting up to 40 s (5120 data points) which is contaminated with eye blink artifacts. The aim of the experiment was to produce data that consists of normal eye activity in order to determine the blink detection rate of the blink detection algorithm as well as the blink correction rate of the wavelet neural network (WNN) blink correction algorithm. At the time of the study each subject gave informed consent for the testing. Ethical approval for the research was obtained from the Human Research Committee of Stellenbosch University, ref nr: N13/04/051.

5.1.2 Simulated Data

In order to quantitatively analyse the WNN and the combination of the blink detection and WNN algorithm two different signals were generated using the simulation model discussed in Chapter 4. The first signal is generated with a sampling rate of 256 Hz for 10 s (2560 data points) and is impregnated with three eye blinks at random locations. The second signal is generated at the same sampling frequency, 256 Hz, for 30 s (7680 data points) and is impregnated with 10 eye blinks at random locations. Refer to Table 5.1 for a summary of the simulated signals. The purpose of the simulated data is to determine the correction accuracy of the WNN blink correction algorithm as well as the correction accuracy of the blink detection and correction algorithms combined.

Table 5.1: Simulated signals properties.

Duration (s)	**Number of eye blinks**	**Sampling rate (Hz)**
10	3	256
30	10	256

5.1.3 Motor Imaginary Data

The EEG data recorded during a motor imaginary experiment [58] was obtained from the Berlin Brain Computer-Interface [58] website where data is publicly available. The EEG data was recorded from seven healthy subjects (details of the subject not provided) each partaking in 11 experiments. The data was collected using a 128 channels sampled at a 1000 Hz and band-passed filtered between 0.05 and 200 Hz. During the experiment, subjects were seated in a comfortable chair with arms relaxed on the arm rest. Two, three or six letters appeared on the computer screen for a duration of three seconds. These letters indicated to the individual what action they should imagine i.e. imagine a left hand movement or an auditory sensation. For each action 160-200 trials were recorded. Two types of visual stimulus were used to indicate the required action. First, the letters appeared at a singular point on the screen which minimizes the eye movement and blink artifacts. Second, the letters appeared at random points on the screen promoting eye movement and blink artifacts. Data recorded using the first method was not used due to lack of eye blink artifacts. The data recorded for one subject, using the second method, was used for testing. However, only the first 30 s of the data was used to decrease the computational load. The purpose of the motor imagery data is to validate the combined blink detection and WNN blink correction algorithm on real EEG data.

5.1.4 Motor Movement Data

The motor movement EEG data was recorded at the University of Cape Town Biomedical Engineering lab using the Net station amplifier and software. The data was collected from two healthy subjects, one male (24 years of age) and one female (23 years of age), using a HydroCel Geodesic Sensor Net with 128 channels and sampled at 500 Hz. It was only possible to test two subjects using Net station due to the equipment being off the premises, software conflicts, and time constraints.

During testing, each individual was seated in a comfortable chair with their arms relaxed on the arm rest and asked to blink normally. For a duration of three seconds one of 4 instructions appeared on the screen followed by a rest period of 1.5 s. During the 3 s period the user either extended his left arm, extended his right arm, rotated his left hand, or rotated his right hand, then returned to the relaxed position until the next instruction appeared. The instructions were carried out sequentially, one after the other, and each instruction was repeated producing 15 trials per instruction, 60 trials in total per subject. This experiment produced data of 270 s (135000 data points). The purpose of the motor movement dataset is to validate the overall process of the algorithms as well as determine the impact eye blink artifacts has on the EEG channels located over the motor cortex. At the time of the study each subject gave informed consent for the testing. Ethical approval for the research was obtained from the Human Research Committee of Stellenbosch University, ref nr: N13/04/051.

5.2 Data Pre-Processing

During data acquisition there are external sources that contribute to diminishing the EEG quality, discussed in Section 2.4, thus, it is important to inspect the data for any artifacts that can alter the final outcome of the experiment. Due to the primary and secondary objective of the thesis (see Section 1.2) only a miniscule amount of data is allowed to be removed from the EEG datasets in order to keep the dataset as close to the original as possible. Thus, the results for the second objective will be more accurate. Therefore, during the pre-processing step only corrupted channels and line noise artifacts were chosen to be removed. Artifacts such as muscle corruption, eye movement, EKG, etc. were ignored due to the assumption that each will be separated into their own independent source component after ICA is applied to the EEG data and will not be part of the eye blink independent source component.

5.2.1 Corrupted Channels Removal

Visual inspection is a common manual artifact detection method used to identify trials and channels that are affected and should be removed from the analysis. In order to determine whether a channel was corrupted its' amplitudes were compared to that of an eye blink. If the amplitudes where greater than that of the eye blink the channel was removed from the study. Each trial of the blink data was inspected and no corrupted channels where found for both subjects. However, for the motor movement data, subject two channel 113 was removed due to corruption whereas subject one had no corrupted channels. The motor imaginary data was pre-processed before it was made available to the public and no information was provided.

5.2.2 Filtering

The desired EEG activity takes place between 0 and 100 Hz. Thus, motor imaginary and movement datasets were filtered using a low pass FIR filter with a cut off frequency of 100 Hz and the blink data was passed through a low pass FIR filter with a cut off frequency of 30 Hz, due to its low sampling frequency of 128 Hz, in order to remove unwanted frequency bands. Both motor imaginary and movement data was passed through a notch FIR filter (cut off frequency of 45 and 55 Hz) in order to remove the external power line noise present in the data.

5.3 Algorithm Implementation

The combination of algorithms was implemented in the MATLAB [59] environment with an additional open source toolbox known as EEGLAB [60]. EEGLAB is provided by the Swartz Center for Computational Neuroscience and provides basic processing tools such as ICA implementation, time/frequency analysis, artifact rejection, as well as other data visualization modes. This section describes the complete process of the algorithms and then explains each key step (detection and correction) in detail.

5.3.1 Overall Process of Algorithms

The overall process of creating artifact free EEG data consists of different algorithms, discussed in Chapter 3, integrated together to take advantage of each algorithm's strength. The complete process, shown in Figure 5.1, consists of several steps and is a combination of manual and automatic processing.

The raw EEG data, acquired from recorded sessions (see Section 5.1), is imported into EEGLAB where the data is pre-processed (see Section 5.2). The

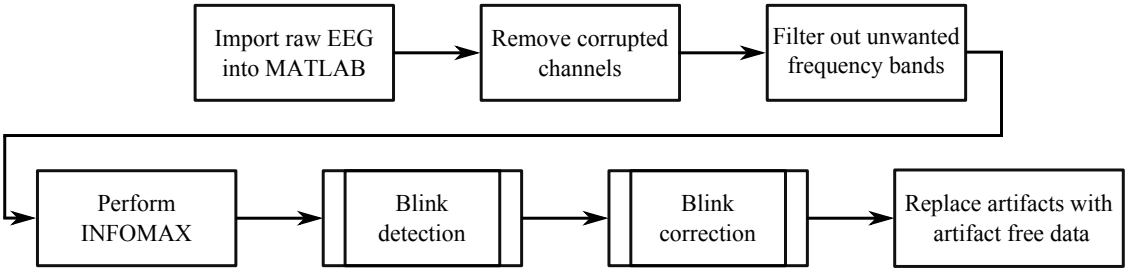

Figure 5.1: Flow chart of overall detection and correction process.

pre-processed data is decomposed using INFOMAX, refer to Table 5.2 for INFOMAX parameters, into independent source components forcing all blink artifacts into a single source component. However, the independent source component containing the eye blink artifacts must still be identified. This is accomplished by visual inspection of each independent source component then manually marking the independent source component containing the eye blink artifact.

Table 5.2: Summary of INFOMAX specifications

Preprocessing	Centering and Whitening
Cost function	Negentropy
Stopping criteria	1E-7

Each eye blink present in the marked independent source component is detected using the blink detection algorithm which is based on wavelet transform. Afterwards the detected blinks are exported in 1 s windows and corrected using a combination of wavelet transform and artificial neural networks known as a wavelet neural network (WNN). The corrected blinks, contained in 1 s windows, are imported and replaces the eye blinks present in the independent source component. This produces an artifact free source component which is used to reconstruct all the EEG data in order to produce artifact free EEG. For an ideal case of ICA a source is generated that contains purely blink artifacts and no underlying neural activity is present, this however is not the case because a vast amount of electrodes are required to determine all the sources. Thus during blink detection only a 1 s portion of data containing the blink artifact is exported and corrected which minimizes the amount of neural activity lost.

5.3.2 Blink Detection

The eye blink detection process is shown in Figure 5.2 and is applied to the marked independent source component, obtained through ICA, containing the

blink artifacts where it makes use of wavelet transform to analyse and detect the blinks. The Haar mother wavelet is a step function that is used to determine the state (open or closed) of an eye [14]. When the EEG data is decomposed and the eye state changes from open to close the waveler transform results in a step function with a falling step. Similarly, when the eye changes from close to open the wavelet transform results in a step function with a rising edge. This allows for precise detection of eye blink artifacts.

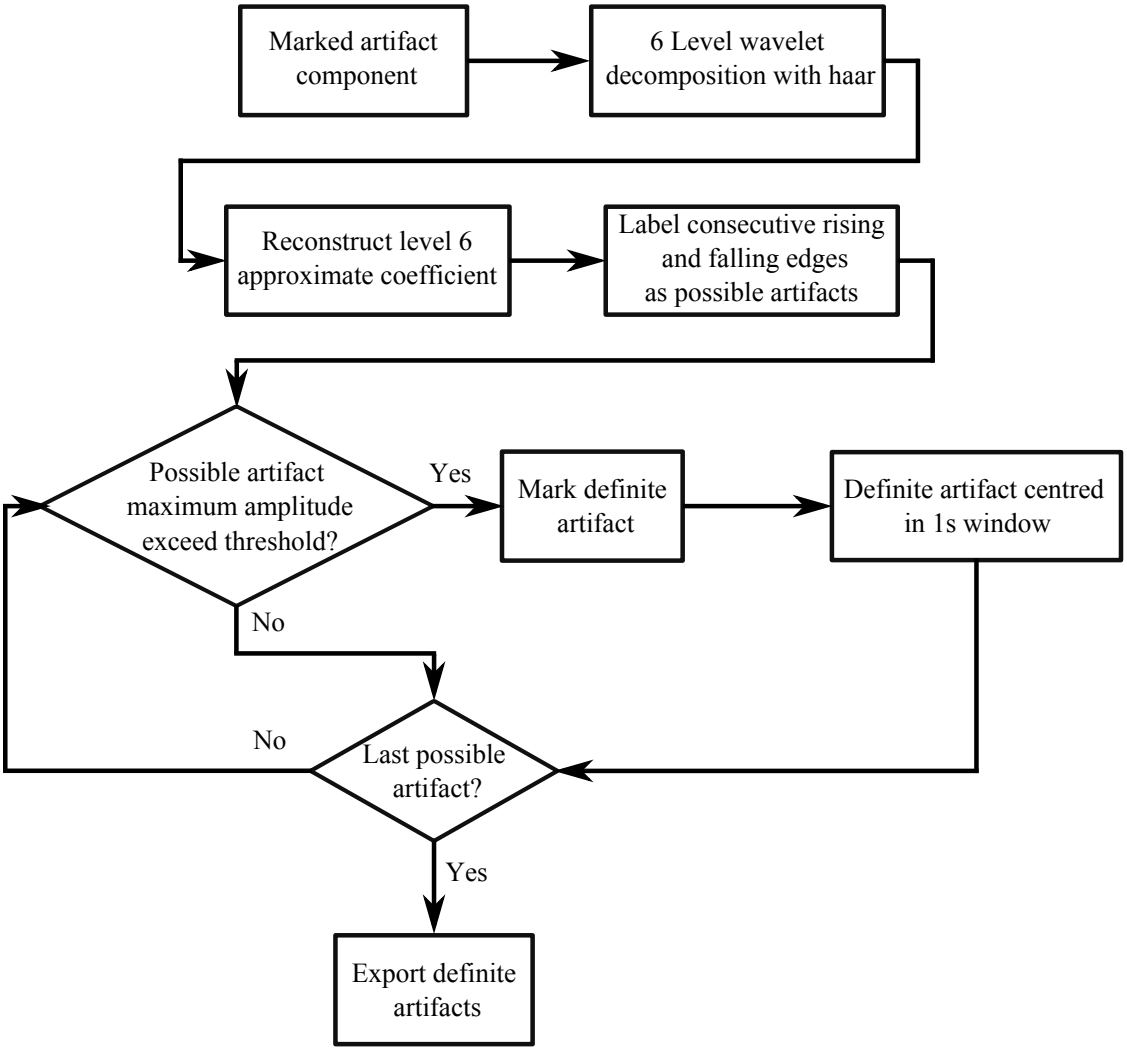

Figure 5.2: Flow chart of eye blink detection algorithm.

The process begins by decomposing the entire marked independent source component (Figure 5.4(a)) to level six using a Haar mother wavelet. Decomposing the independent source up to six levels forces the eye blink artifact data into the approximate coefficient frequency band (at level six) thus reducing the amount of high frequency data allowing only the high amplitude low frequency

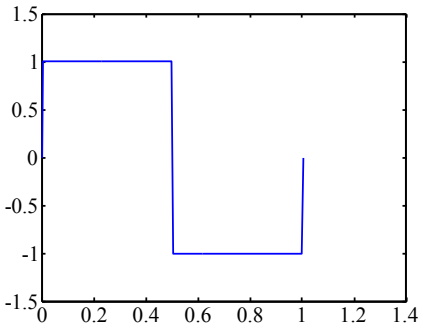

Figure 5.3: Haar wavelet [59].

data to be reconstructed. After signal decomposition a series of detailed and approximate frequency bands are produced where only the approximate frequency band of the decomposed signal is reconstructed at the 6th level (Figure 5.4(b)), producing a series of step functions, and each consecutive rising and falling edge is marked as a possible artifact. The maximum magnitude of the original independent source component, within the rising and falling edge indices, are compared to a manually set threshold (Figure 5.4(c)). Through visual inspection the threshold TH was defined as

$$TH = \frac{1}{3}\left(\frac{\sum_1^O OA_{MAXo}}{O}\right) \tag{5.3.1}$$

where O is the total number of eye blinks in the independent source component and OA_{MAXo} is the maximum magnitude of o eye blink. Thus the threshold is a third of the average amplitude of eye blinks in the independent source component. The threshold function is applied to each new independent source component to adjust the threshold in order to maintain maximum detection rates for each case. After threshold comparison, each possible artifact, that fails the threshold test, is marked as a definite artifact. After a possible artifact is marked as a definite artifact, its maximum amplitude is centred in a 1‘s window (Figure 5.4(d)) and then exported to the WNN for further processing. The window size of 1 s was chosen because it allows an error margin of 300 ms on either side of the blink allowing any outlier cases, eye blinks longer than 200 to 400 ms, to still be captured within the window. It also provides enough data points for the neutral network to process.

5.3.3 Wavelet Neural Network

The wavelet neural network is a combination of wavelet transform and artificial neural networks proposed by Nguyen et al. [15]. This combination takes advantage of wavelet transform's ability to match a wavelet to the eye blink artifact, through compressing, stretching, and scaling of the wavelet, with great time resolution. This approach also makes use of the artificial neural network's ability to generalize and learn to identify or correct outlier information such

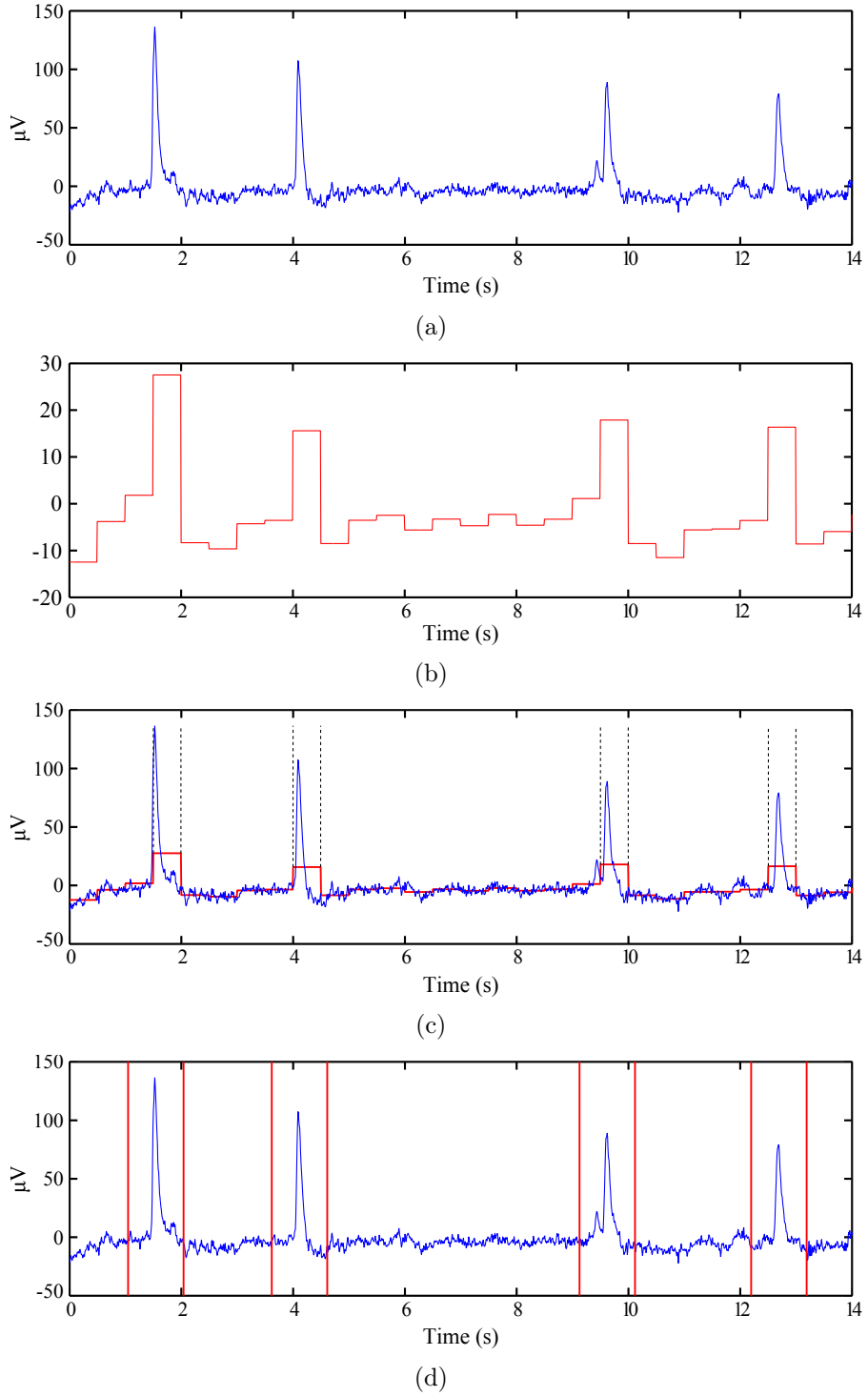

Figure 5.4: Illustration of eye blink detection where a) the signal is decomposed, b) reconstruction of approximate coefficients, c) determining maximum blink magnitude, and d) centring eye blink in 1s data segment.

as artifacts. The structure of the wavelet neural network consists of the generated coefficients (approximate and detailed) as well as the neural network. The study focused on two different models for the wavelet neural network. For both models the input data is normalised and the output layer has a hyperbolic tangent sigmoid transfer function. However, each model has a different structure. Model 1 consist of a 1-6-1 (1 input unit, 6 hidden layers, and 1 output unit) neural network where only the lowest frequency band, approximate coefficients, are processed, see Figure 5.5(a). Model 2 consists of a 3-6-3 (3 input unit, 6 hidden layers, and 3 output unit) neural network where the 3 lowest frequency bands, approximate and detailed coefficients, are processed, see Figure 5.5(b).

Due to the high level of wavelet decomposition (discussed in the next section) it was uncertain whether the eye blink artifact data will be forced into only the approximate frequency band or distributed among the lowest frequency bands, thus two models are investigated. Both models' training and blink correcting procedure are identical and will be discussed next.

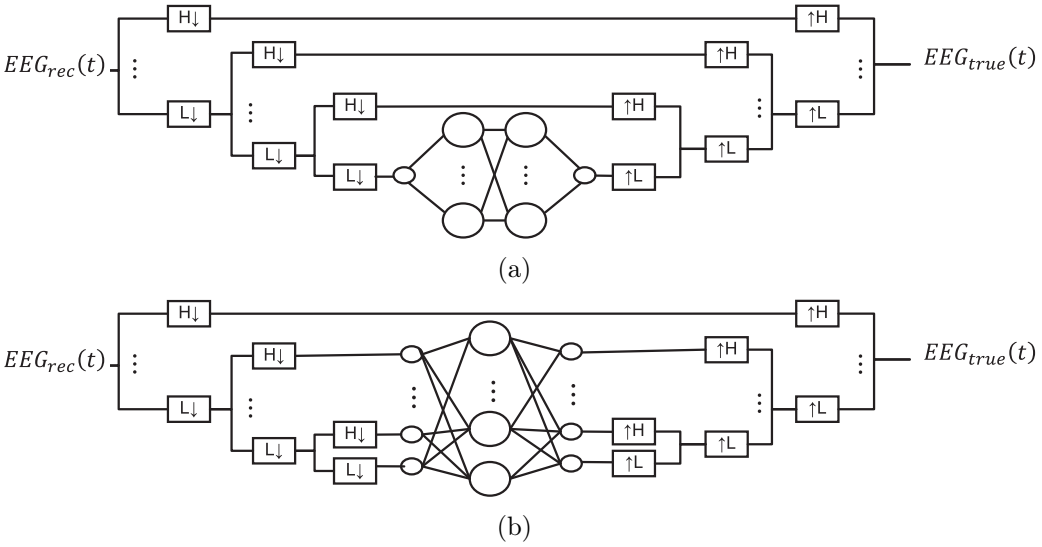

Figure 5.5: Wavelet neural network structure of a) model 1 and b) model 2 (adapted from [15]).

5.3.3.1 Training

In order to utilize this algorithm it must be trained to recognise the eye blink artifact coefficients and correct them. The neural network is trained using a supervised method known as resilient backpropagation (see Section 3.3.3) which requires sample inputs and the desired outputs for the sample inputs.

Using the EEG signal simulation model, described in Chapter 4, a 30 s artifact free and artifact containing signal, which contains 10 eye blink artifacts, is generated. Each eye blink artifact (sample inputs) as well as its artifact free counterpart (desired output) is extracted in 1 s windows using the blink detection method described in Section 5.3.2. Following the training process shown in Figure 5.6 both models are trained per eye blink and each eye blink is repeated 200 times which results in 2000 training sessions per model. The repetition training of an eye blink is done to ensure that the neural network does not stick to one local minima for performance but explores all options.

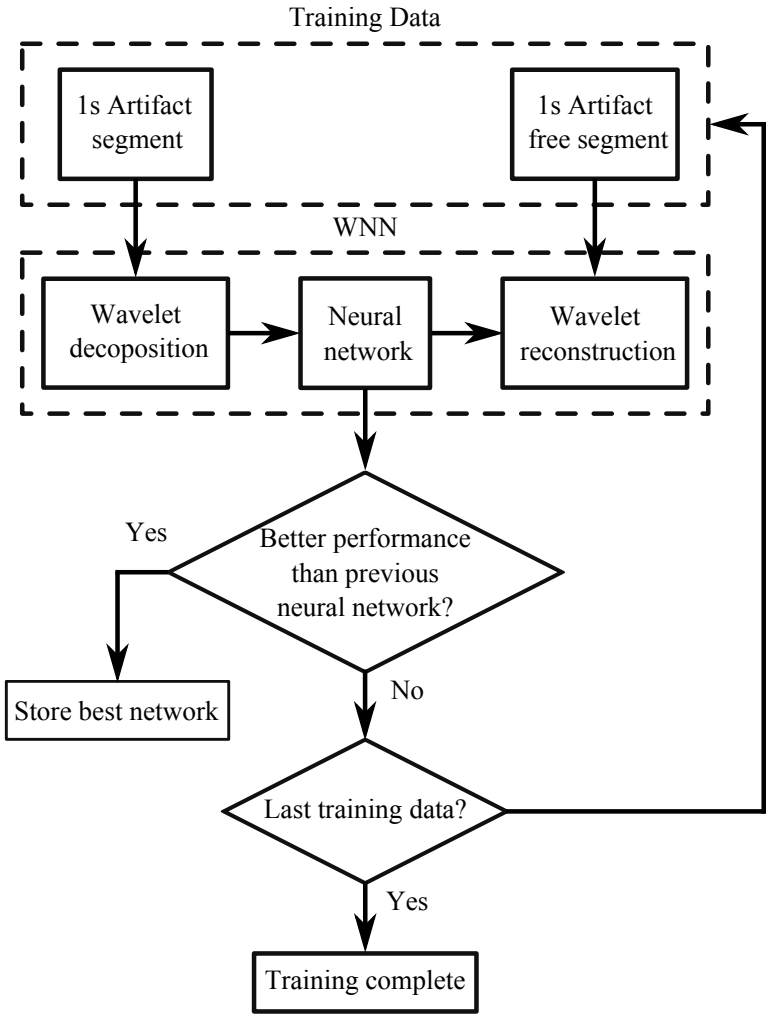

Figure 5.6: Flow chart of training procedure for neural network.

The sample input and target output is decomposed to level eight using a 3rd order coiflet mother wavelet [15]. The 3rd order coiflet wavelet was chosen due to the resemblance it has with an eye blink, see Figure 5.7. Decomposing the independent source up to eight levels forces the eye blink artifact data further

into the lower frequency band thus reducing the amount of high frequency data, more than that of a level six decomposition, allowing only the high amplitude low frequency data to be present. Thus, for model 1's input only the level eight approximate low frequency coefficient band is used, whereas for model 2's input the level eight approximate and level seven and eight detailed frequency coefficient band is used. The inputs of both models are interpolated to ensure the same vector size. Using resilient backpropagation the network is trained so that the output of the network matches the target output. Only 70 % of the eye blink data points were used for training the neural network, the remainder was used to validate and test the neural network in order to determine its performance. This process is repeated for all 10 eye blink artifacts and the network with the best performance is used for correcting eye blink artifacts. The neural network training parameters used for model 1 and 2 are shown in Table 5.3.

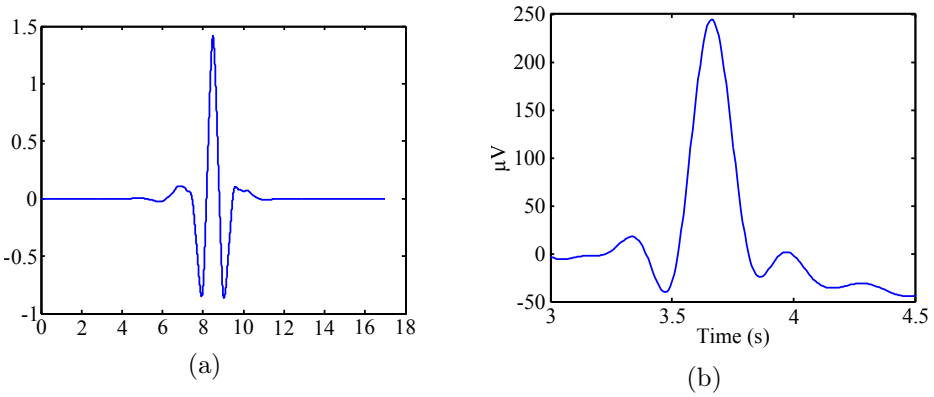

Figure 5.7: The waveform of a) 3rd Order coiflet wavelet [59] and b) eye blink artifact.

Eye blink artifacts all have the same morphology for each individual thus the WNN training procedure is carried out once to achieve the optimal WNN. This reduces the processing time of the procedure because no changes or preparations has to be made for the next data set.

5.3.3.2 Blink Correction

After the blink detection algorithm 1 s data segments containing the eye blink artifact is exported to and processed by the optimal WNN. The blink correction procedure, see Figure 5.8, corrects each data segment separately. The artifact segment is decomposed to level eight using a 3rd order coiflet wavelet, the same as the training procedure, to produce approximate and detailed coefficients. The coefficients are interpolated (ensuring same vector sizes) and,

Table 5.3: Summary of neural network training parameters

	Model 1	**Model 2**
Training method	Resilient backpropagation	Resilient backpropagation
Maximum iterations	2000	1000
Maximum validation failures	100	6
Minimum performance gradient	1E-6	1E-6
Data division	Training: 70 %	
	Validation: 15 %	
	Testing: 15 %	

depending on the model, either the level eight approximate frequency coefficients band or the level eight approximate and level seven and eight detailed frequency coefficients band are the inputs of the neural network. After correcting the outlier artifact coefficients the approximate and detailed coefficients are downsampled to their original vector sizes and combined with the remaining unprocessed detailed coefficients to reconstruct the 1 s data segment which is artifact free. The artifact free 1 s data segments is returned to the independent source component, only replacing its corresponding artifact segment.

5.4 Evaluation Methods

In order to determine whether this method is successful the performance of the overall process as well as the individual parts must be studied. In this section the methods used to evaluate the algorithms are discussed.

5.4.1 Power Spectral Density

In order to fully comprehend the degree to which the corrected signals resembles the input signals, in the frequency domain, the signals were evaluated using power spectral density (PSD). Using a nonparametric method known as Welch, which is based on averaging the periodogram spectrum with overlapping windows, the frequency content of the segments were evaluated.

5.4.2 Frequency Correlation

In order to fully grasp the changes that occurs in the independent source components, after blink correction, as well as the overall EEG signals one must investigate the relationship between the original signal and the corrected

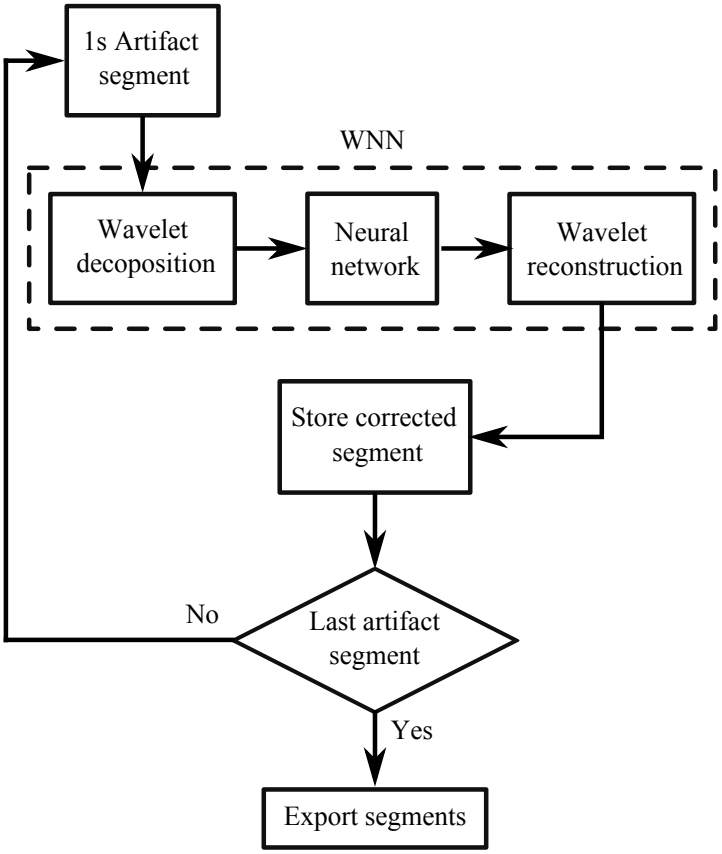

Figure 5.8: Flow chart for blink detection process.

signal. Frequency correlation [61] determines the relationship between two signals and reduces it to a single constant. If the constant is 0 the signals are not related but if it is 1 the signals are identical. Using frequency correlation (FC) the mutual relationship between two signals can be determined.

5.4.3 Root Mean Square Error

To determine how accurate a system is the output as well as the desired output must be known. Thus, using root mean square error (RMSE) and the simulated signals (see Section 5.1.2) the accuracy of the algorithms can be determined. RMSE determines the difference between signals in the time domain by squaring the distance between each point of the signal and taking the square root of the average distance. Thus the smaller the RMSE value, the smaller the difference is between the two signals [15].

5.5 Testing Procedure

In this section the testing procedure is discussed for each algorithm as well as the overall process of the algorithms.

5.5.1 Blink Detection

The blink dataset, after pre-processing, was used to test the blink detection algorithm to determine its detection rate. Each 40 s trial, for both subjects, containing eye blinks was first decomposed into independent source components. The independent source component as well as the total number of eye blinks present in the source component was determined using visual inspection. Afterwards each trial marked independent source component was passed through the blink detection algorithm and the number of blinks detected and the total blinksd present was recorded, refer to Appendix A.

5.5.2 WNN Blink Correction

The simulated dataset was used to quantitatively analyse the correction ability of the WNN blink correction algorithm. Newly generated 30 s simulated signal containing 10 eye blink artifacts was passed through the blink detecting algorithm in order to produces ten 1 s signal segments each containing an eye blink. This is done because the WNN was trained with a 1 s segment of data. Each 1 s segment was passed through the WNN and the resulting 1 s segment was evaluated using the evaluation methods described in Section 5.4.1 and 5.4.3. The purpose of the test was to evaluate the WNN blink correction as well as determine its accuracy.

5.5.3 ICA and WNN Blink Correction

The purpose of the testing was to determine how well the combined algorithms, blink detection and correction, correct an eye blink artifact independent source component. Three different datasets were used to quantitatively analyse the combined algorithms, determine their performance on true EEG data, and determine their correction rate.

To analyse the combined algorithms quantitatively the simulated dataset was used. The 10 s simulated signal, representing an independent source component, containing three eye blinks was firstly passed through the blink detection algorithm. The detected eye blinks were exported, in 1 s segments, from the simulated component and passed through the WNN blink correction algorithm. After each 1 s segment was corrected the eye blinks present in the simulated component were replaced by their corresponding corrected segment producing an artifact free independent source component. The corrected artifact

independent source component was evaluated using the evaluation methods in Section 5.5.

The motor imaginary dataset was used to determine the combined algorithm's perform with real EEG data. The 30 s signal of one subject was decomposed into independent source components using ICA. The independent source component corrupted with eye blink artifacts was marked and passed through the blink detection algorithm. All the detected blinks were extracted in 1 s segments and passed through the WNN blink correction algorithm. After each 1 s segment was corrected the eye blinks present in the marked independent source component were replaced by their corresponding corrected segment producing an artifact free independent source component. The corrected artifact independent source component was evaluated using the evaluation methods in Section 5.5.

In order to determine the correction rate for the combined algorithms the total artifacts present in the dataset and the total amount of artifacts detected had to be known, thus the blink data was used. The 1 s segments of detected eye blinks (see Section 5.5.1), for each trial, was passed through the WNN blink correction. The resulting corrected segments mean amplitude was visually compared to the amplitude of the signal before and after the eye blink as well as the eye blinks amplitude. The segments that were corrected successfully, mean amplitude resemble the amplitudes of the signal before and after the eye blink, was rated 1 whereas the segments that were not successfully corrected, mean amplitude resembles the eye blink amplitude, was rated 0, refer to Appendix A.

5.5.4 EEG Blink Correction

The motor movement dataset was used to evaluate the overall process of the combined algorithm. The 270 s EEG data, for both subjects, was decomposed into independent source components using ICA. The independent source component corrupted with eye blink artifacts was marked and passed through the blink detection algorithm. All the detected blinks were extracted in 1 s segments and passed through the WNN blink correction algorithm. After each 1 s segment was corrected the eye blinks present in the marked independent source component were replaced by their corresponding corrected segment producing an artifact free independent source component. Afterwards all the independent source components including the corrected component are recombined to create artifact free EEG signals. Channels F_z , C_4, and C_3 were evaluated using the evaluation methods in Section 5.5 to verify the primary and secondary objective.

Chapter 6

Results

In this chapter the experimental results obtained from using the combined algorithms to remove eye blink artifacts are discussed.

6.1 Blink Detection

From the testing procedure explained in Section 5.5.1 results were produced indicating the detection rate of the blink detection algorithm. The complete set of results (refer to Appendix A) demonstrate the number of eye blinks detected, the number of undetected blinks, and the true amount of eye blinks as well as the overall performance. Table 6.1 provides a summary for both subject's data sets where eye movements vary in each recording session. Subject 1 achieved a successful detection rate of 88.2 % and subject 2 achieved a successful detection rate of 93 %. Overall, a successful detection rate of 90.4% was achieved.

Table 6.1: Summary of eye blink detection rate for subject 1 and 2.

	Eye blinks detected	**Eye blinks not detected**
Subject 1	88.2%	11.8%
Subject 2	93 %	7 %
Average	90.6 %	9.4 %

6.2 WNN Blink Correction

From the training procedure, explained in Section 5.3.3.1, and the testing procedure, explained in Section 5.5.2, results were produced demonstrating the WNN's ability to correct a 1 s segment of data containing a single eye blink artifact.

6.2.1 Training Results

Figure 6.1 shows the results of the WNN training for model 1 and 2. The WNN used the sample input (green line) and adjusted the network weights to ensure the output (red line) of the network is as close to the target data (blue line) as possible. Figure 6.1(a) and 6.1(b) shows each model's 1 s training segment that produced the best results.

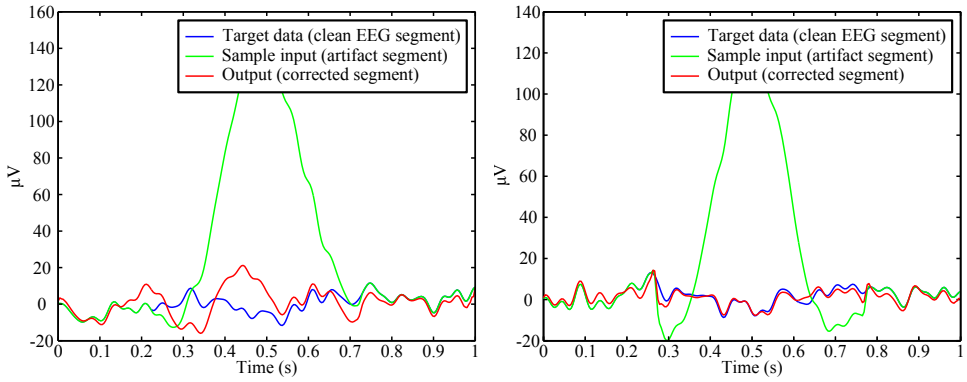

Figure 6.1: Training data for a) model 1 and b) model 2.

In order to fully comprehend the degree to which the actual output resembles the target output the 1 s training segments were evaluated in the frequency domain using PSD. Figure 6.2 shows the PSD analysis (see Section 5.4.1) of the 1 s training segments for model 1 and model 2.

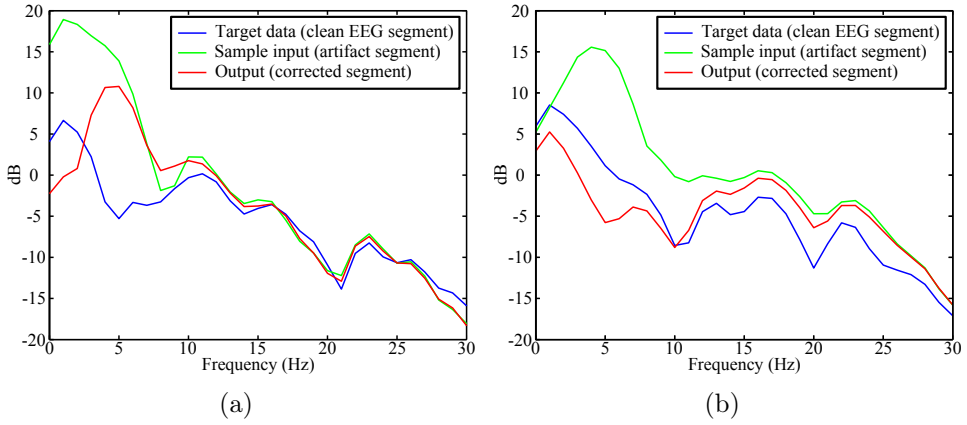

Figure 6.2: PSD of training data for a) model 1 and b) model 2.

The sample data (green line) represents the typical shape of an eye blink infected segment where the large peak between 0 and 5 Hz is produced by the large magnitude of the blink. The target data (blue line) which contains no large peak represents the artifact free data where the actual output (red line) represents the correction made by compressing the eye blink in the frequency domain.

To further assist in determining the accuracy of the models the RMSE (see Section 5.4.3) was determined between the 1 s corrected segment and the 1 s target segment (clean EEG segment). Table 6.2 shows the RMSE values for both models' 1 s training segment.

Table 6.2: Training datas RMSE values for model 1 and 2.

	Model 1	**Model 2**
Best segment	8.6605	2.1570

6.2.2 Testing Results

Figure 6.3 shows one of the 1 s segments used to test both WNN models. The corrected 1 s segment (red line) was produced by correcting the artifact 1 s segment (green line) which closely resembles the actual artifact free 1 s segment (blue line).

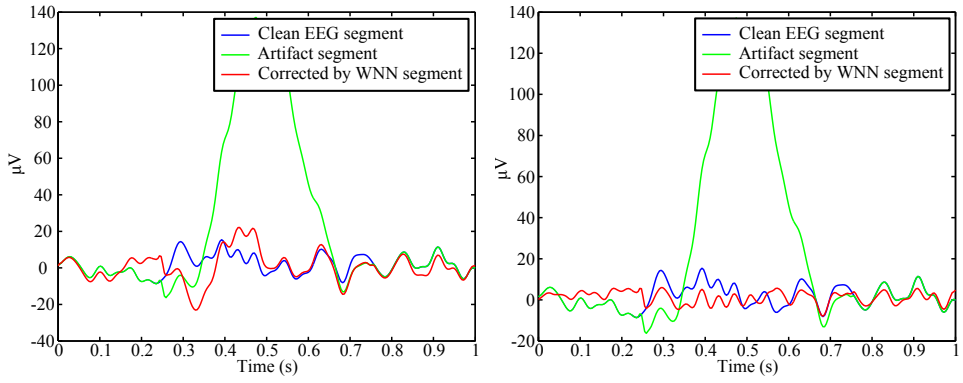

(a) (b)

Figure 6.3: Testing data for a) model 1 and b) model 2.

The PSD seen in Figure 6.4 shows the 1 s artifact segment (green line), where the peak between 0 and 5 Hz represents the artifact in the 1 s segment, being

compressed (corrected) resulting in the corrected 1 s segment (red line). From Figure 6.2 and 6.4 it's observed that the WNN overcorrects the low frequency band data instead of only correcting the artifact data.

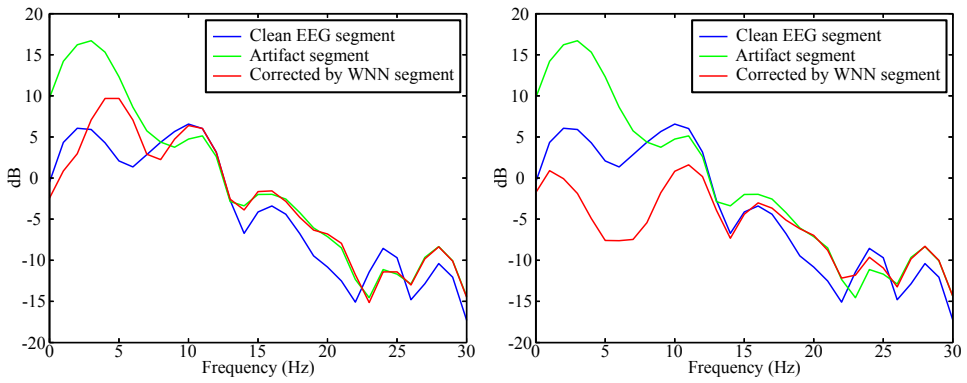

Figure 6.4: PSD of testing data for a) model 1 and b) model 2.

Table 6.3 shows the RMSE values for each testing 1 s segment as well as the average of all 10. Segment 6 of model 2 contained large low frequency activity and thus produced an outlier RMSE value of 11.9669 which further confirms the over correction of low frequency bands.

Table 6.3: Testing segments RMSE values for model 1 and 2.

Segment	**Model 1**	**Model 2**
1	9.0746	5.6967
2	8.7547	7.8000
3	6.8660	7.9848
4	8.4214	9.1045
5	9.1661	9.8937
6	7.7218	11.9669
7	7.2954	7.7422
8	7.9808	4.2721
9	5.6763	5.3739
10	6.8651	5.3739
Average	7.7813	7.5421

6.3 ICA and WNN Blink Correction

From the testing procedure, explained in Section 5.5.3, results were produced demonstrating the combined ability of the blink detection and WNN blink correction algorithm to correct independent source components that contain eye blink artifacts.

6.3.1 Simulated Dataset

Figure 6.5 shows the results obtained for both models by correcting a simulated independent source component one. The original independent source component (green line) stays unchanged for the time range until an artifact occurs which produces a large amplitude. The corrected independent source component (red line) shows that the changes made to the original independent source component are focused only on the time range that the artifact occurs.

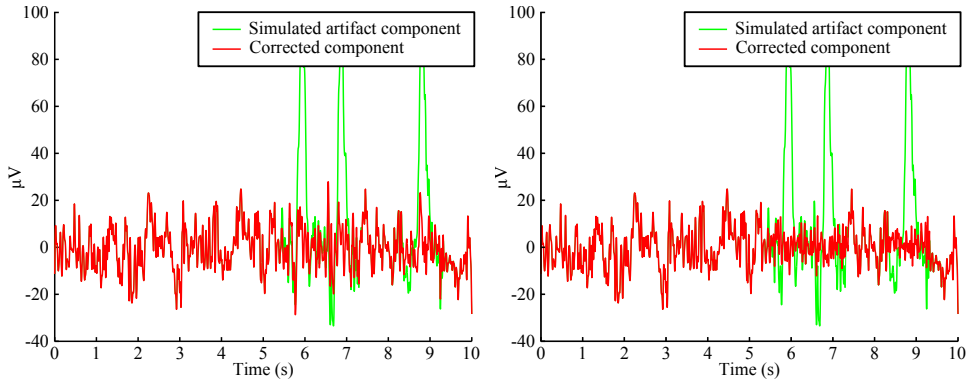

Figure 6.5: Simulated contaminated independent source component corrected by a) model 1 and b) model 2.

Figure 6.6 shows the PSD, for both models, of the simulated artifact independent source component (green line) and the corrected independent source component (red line). Altering only a segment of the signal that contains the artifact minimizes the loss or error in the correction process thus producing a similar PSD as the original simulated artifact free independent source component (blue line).

Figure 6.7 shows the frequency correlation for both models. In Figure 6.7(a) the relationship between the corrected simulated independent source component and the artifact free simulated independent source component is shown for model 1.

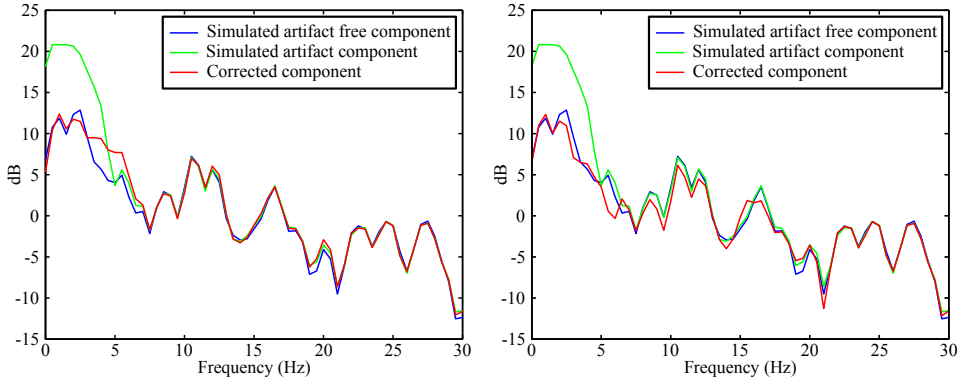

Figure 6.6: PSD of simulated contaminated independent source component corrected by a) model 1 and b) model 2.

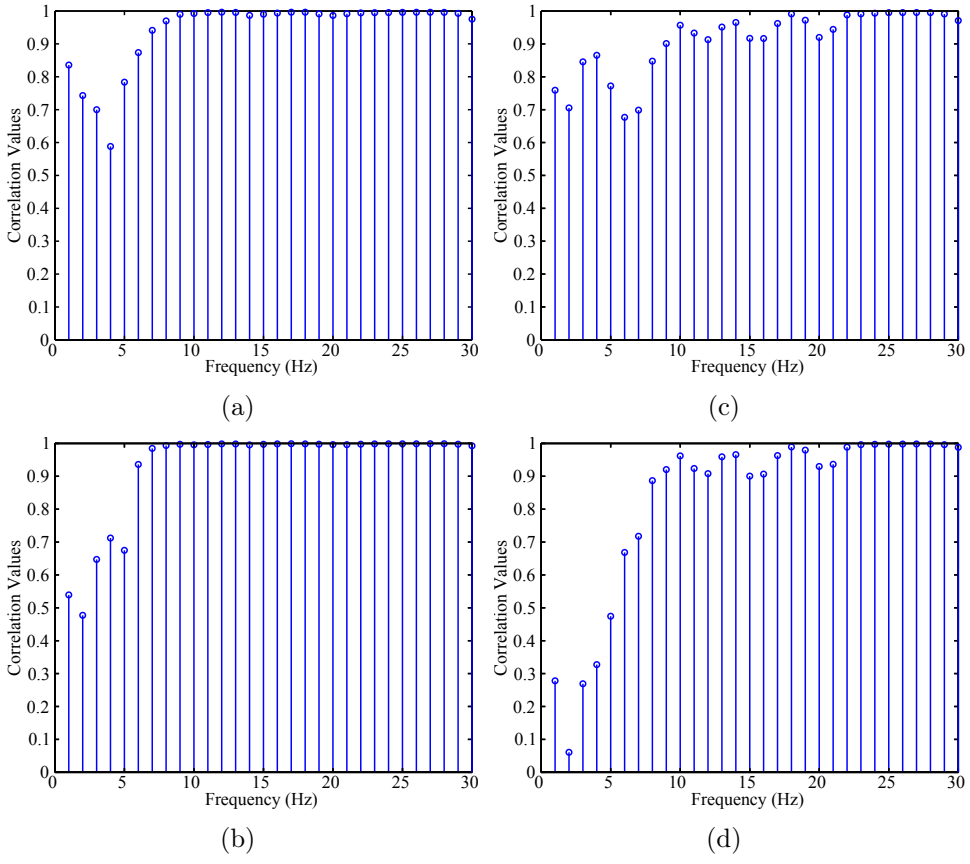

Figure 6.7: Frequency correlation of model 1 for a) corrected source component vs. artifact free source component b) corrected source component vs. artifact source component and model 2 for c) corrected source component vs. artifact free source component d) corrected source component vs. artifact source component.

Between 0 and 10 Hz it is clear there is a difference between the corrected simulated independent source component and the artifact free simulated independent source component where above 10 Hz the corrected simulated independent source component is identical to the artifact free simulated independent source component. The relationship between the corrected simulated independent source component and the artifact simulated independent source component for model 1, see Figure 6.7(b), shows the same relationship as Figure 6.7(a). However, the difference between the corrected and artifact simulated independent source component is greater (closer to 0) in the low frequency band than Figure 6.7(a) which indicates that low frequency information was changed. For model 2 the same results are obtained, see Figure 6.7(c) and 6.7(d). However small changes occur between 10 and 20 Hz which is caused by model 2's structure which corrects 3 coefficients bands instead of just one as is the case with model 1.

Table 6.4 shows the RMSE values for each testing independent source component as well as the average of all 10. Component 1 of model 2 overcorrected the eye blink artifact which resulted in an RMSE value of 5.3256.

Table 6.4: Testing simulated independent source components RMSE values for model 1 and 2.

Simulated component	**Model 1**	**Model 2**
1	5.2931	5.3256
2	3.9077	2.7179
3	3.8429	2.7895
4	3.6931	3.5860
5	3.3928	3.2118
6	4.7980	3.1978
7	3.7641	3.2383
8	3.6025	2.9233
9	3.7716	3.2167
10	4.4582	3.0084
Average	4.0524	3.3215

6.3.2 Motor Imaginary Dataset

Figure 6.8 shows the result for both models where the contaminated independent source component (green line) is corrected producing the corrected independent source component (red line).

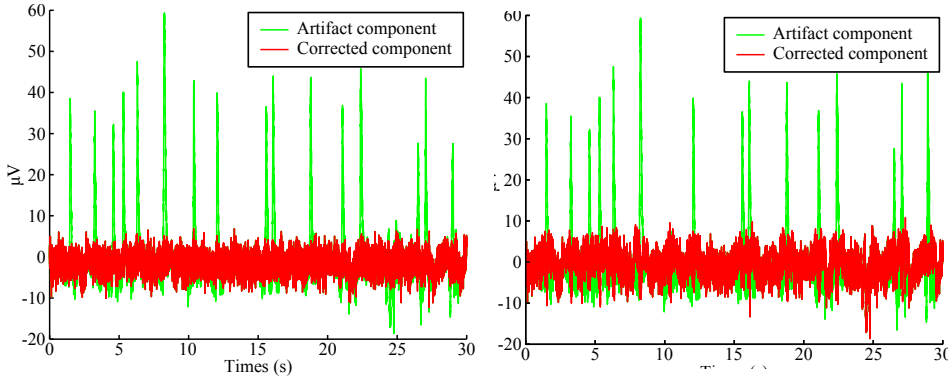

(a) (b)

Figure 6.8: Contaminated independent source component corrected by a) model 1 and b) model 2.

Figure 6.9 demonstrate the changes the algorithm has made to the original signal in the frequency domain. The combined eye blink detection and correction suppress the power in the low frequency band (red line) of the artifact independent source component (green line). Notice after model 2 corrects the independent source component a small increase in power at 15 Hz occurs which is produced during the replacement of the artifact segment with the corrected segment (further discussed in Chapter 7).

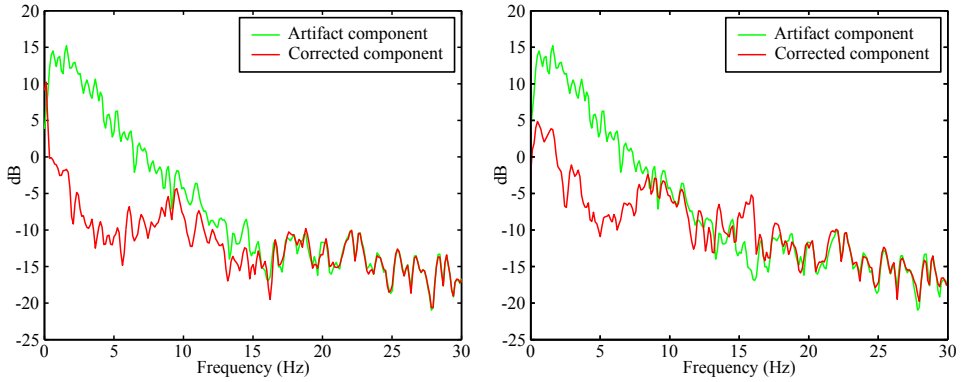

(a) (b)

Figure 6.9: PSD of the contaminated independent source component corrected by a) model 1 and b) model 2.

The frequency correlation of both models, see Figure 6.10, for the corrected independent source component vs. the artifact independent source component

demonstrates that the combined algorithms changes the low frequency information. Figure 6.10(b) shows that at 15 Hz there is a difference in the signal thus confirming the peak produced in Figure 6.9(b).

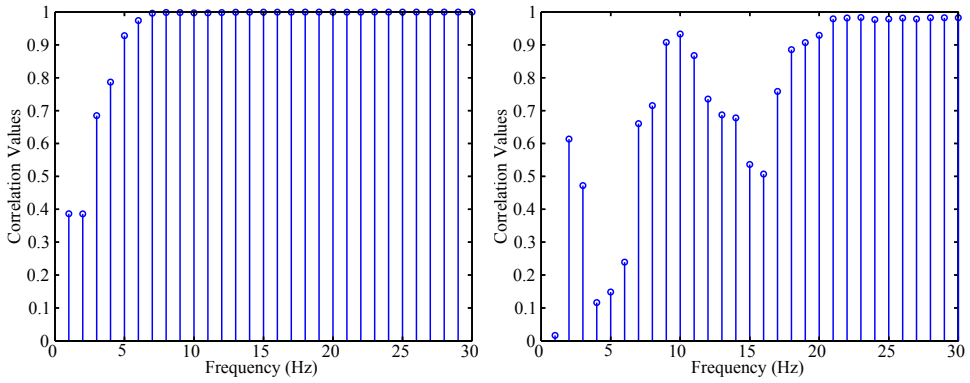

(a) (b)

Figure 6.10: FC of the corrected independent source component vs. contaminated independent source component corrected by a) model 1 and b) model 2.

6.3.3 Blink Dataset

The correction rate of the combined algorithm (blink detection and correction) applied to the artifact independent source component was determined, see Section 5.5.3. Table 6.5 shows a summary of the results obtained for subject 1 and 2. Refer to Appendix A for a complete set of results.

Table 6.5: Summary of eye blink correction rate results for subjects 1 and 2.

	Model 1	**Model 2**
Subject 1	0.7 %	99.3 %
Subject 2	2.3 %	97.2 %
Average	1.5 %	98.3 %

Model 2 produced exceptional results for both subjects resulting in a correction rate of 99.3 % for subject 1 and 97.2 % for subject 2 with an overall correction rate of 98.3 %. However, model 1 produced exceptionally poor results. Subject 1 only achieved a correction rate of 0.7 % and subject 2 achieved a correction rate of 2.3 % with an overall correction rate of 1.5 %. Model 1's poor correction rate is caused by its inability to completely correct the eye blink artifact resulting in a peak slightly smaller than the original eye blink artifact, see

Figure 6.11(c). Figure 6.11(d) demonstrate model 2's ability to fully correct the eye blink artifacts present in the independent source component.

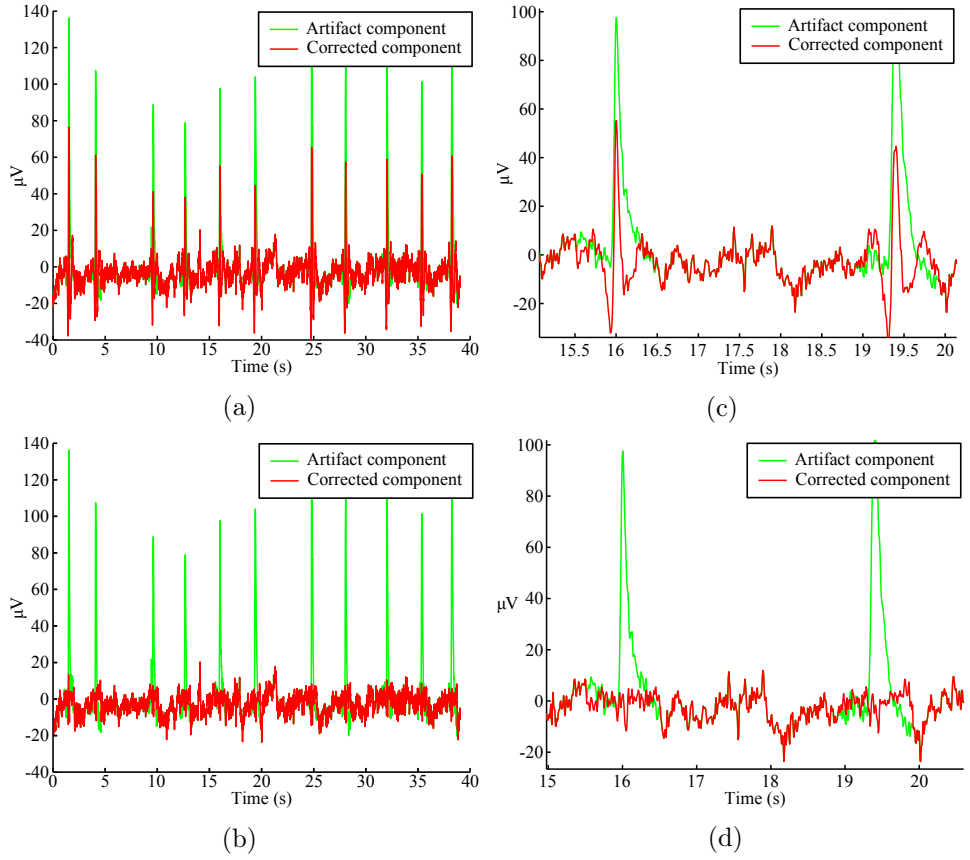

Figure 6.11: Artifact independent source component correction of a) model 1 and b) model 2 with enlarged views between 15 and 20 s for c) model 1 and d) model 2.

6.4 EEG Blink Correction

From the testing procedure explained in Section 5.5.4 results were produced indicating the correction ability of the overall algorithm process. Figure 6.12 shows channel F_z before correction (green line) and after correction (red line) for both subjects. Due to the nature of the study no other artifacts were removed so as to purely determine the correction made, thus eye movement artifacts are still present in the data which is seen in Figure 6.12(a) and 6.12(b) as remaining large spike-like activity. Figure 6.12(c) and 6.12(d) shows more

clearly the eye blink artifact correction made by model 2.

The PSD of both subjects shown in Figure 6.13 demonstrate how the overall process of the algorithm changes the low frequency information. The corrected channel (red line) has an increase in power at 15 Hz which is produced by the replacement of the eye blink artifacts by the corrected artifact (discussed in Chapter 7) and is not part of the original signal (green line).

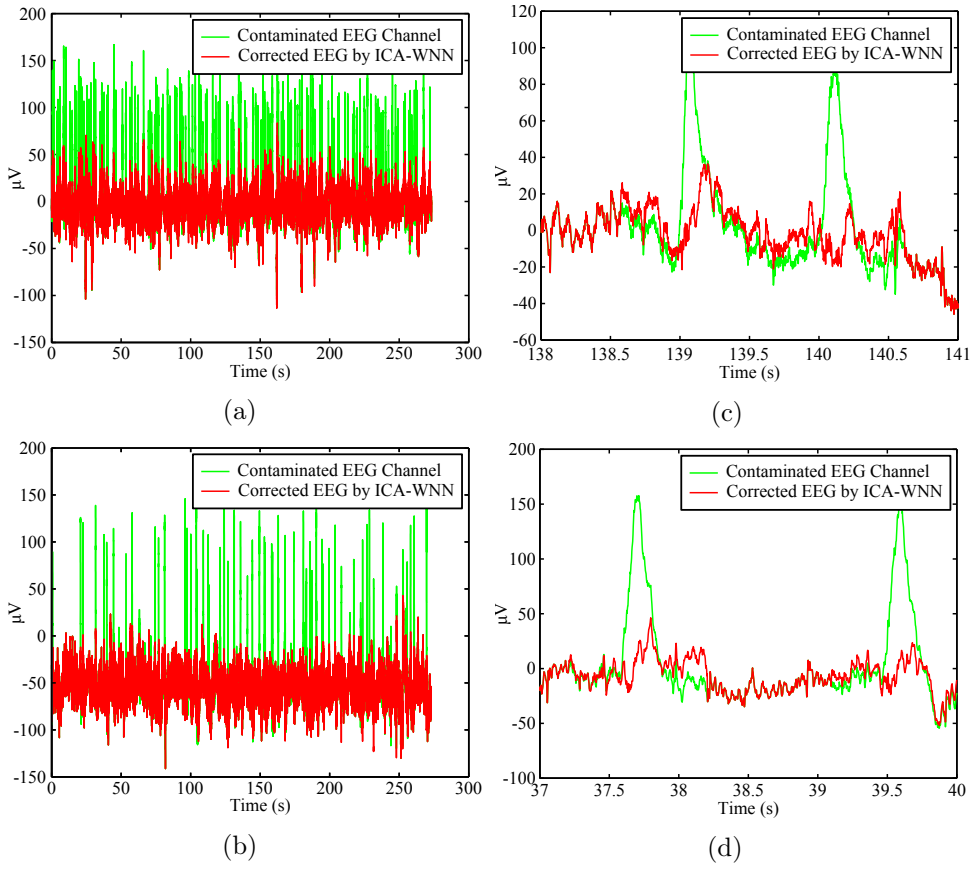

Figure 6.12: Channel F_z artifact correction of a) subject 1 and b) subject 2 with enlarged views between c) 138 and 141 s for subject 1 and d) 37 and 40s for subject 2.

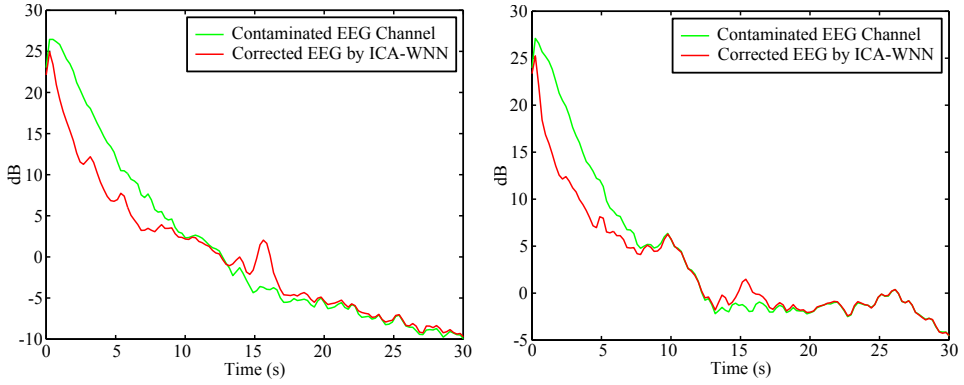

(a) (b)

Figure 6.13: PSD of corrected artifact in channel F_z of a) subject 1 and b) subject 2.

Figure 6.14 demonstrates the frequency correlation of the corrected channel vs. the artifact channel for both subjects which indicates a change of low frequency information. However, subject 1 experienced a large amount of slow wave activity which is over corrected by the WNN due to the vast amount of blink artifacts present in the channel. This causes the frequency correlation in Figure 6.14(a) to decrease to an average of 0.1 between 0 and 5 Hz .

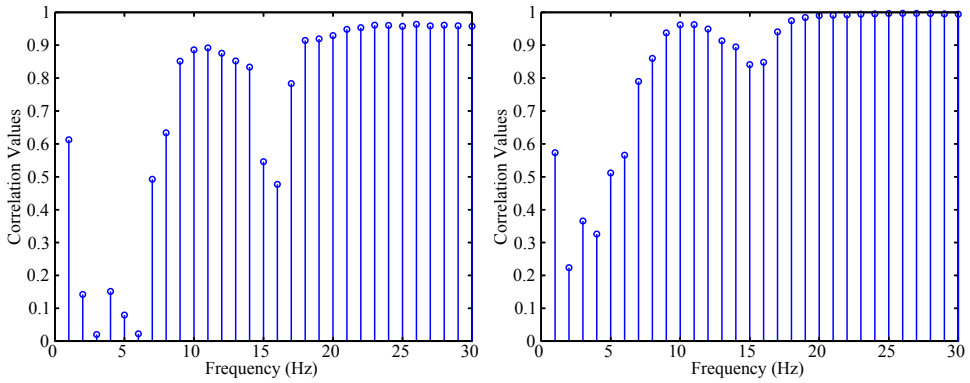

(a) (b)

Figure 6.14: FC of corrected artifact in channel F_z of a) subject 1 and b) subject 2.

In order to investigate the severity of eye blink's effect over the motor cortex, channels located over the cortex must be evaluated. Channel C_3 for both subjects are shown in Figure 6.15 where both corrected (red line) and uncorrected channel (green line) almost have an identical signal. Figure 6.15(a) and 6.15(b), enlarged view, shows that miniscule changes occur in the signal after

artifacts are corrected when compared to Figure 6.12(c) and 6.12(d).

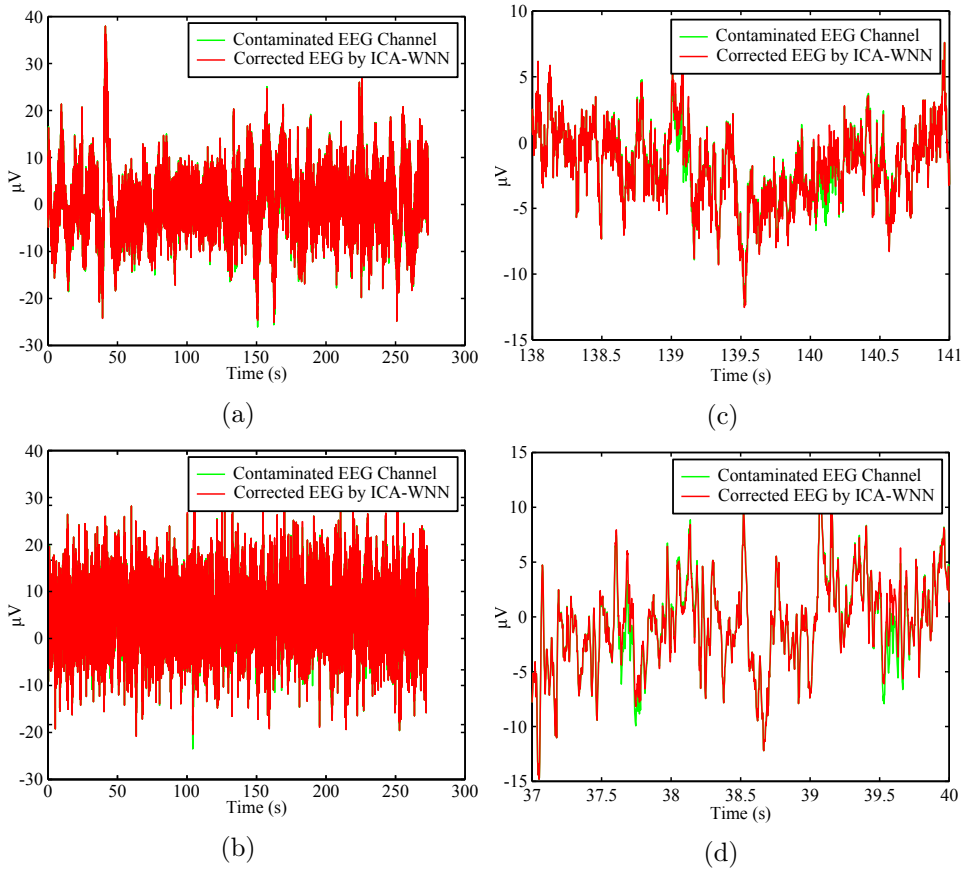

Figure 6.15: Channel C_3 artifact correction of a) subject 1 and b) subject 2 with enlarged views between c) 138 and 141 s for subject 1 and d) 37 and 40 s for subject 2.

The PSD, see Figure 6.16, further confirms the results obtained in Figure 6.15. For both subjects there is a miniscule drop between 0 and 5 Hz in power, so small that it is barely visible. Unlike channel F_z results, the induced 15 Hz increase in power does not affect the C_3, however, there is a peak power between 10 and 15 Hz. This peak, in the alpha range, is generated by motor movement indicating that the subjects were moving during the dataset.

Figure 6.17 further confirms the results, where very little to no change has been made to channel C_3 by the correction algorithm. The frequency correlation shows that the corrected channel is almost identical to the uncorrected channel which indicates miniscule changes were made to the signal.

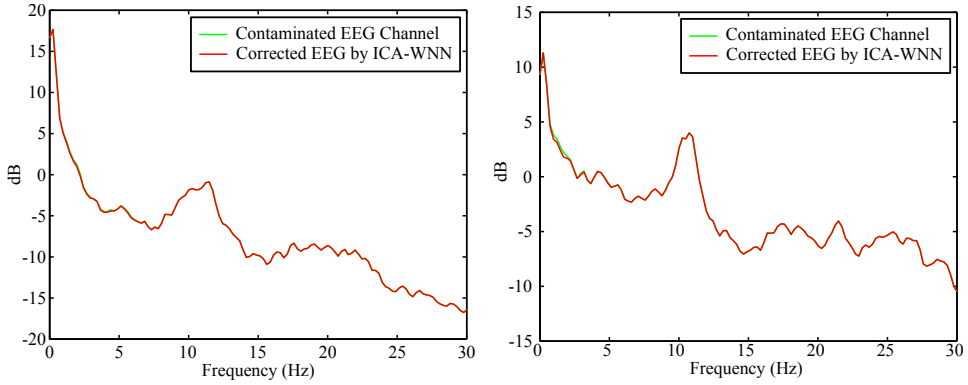

(a) (b)

Figure 6.16: PSD of corrected artifact in channel C_3 of a) subject 1 and b) subject 2.

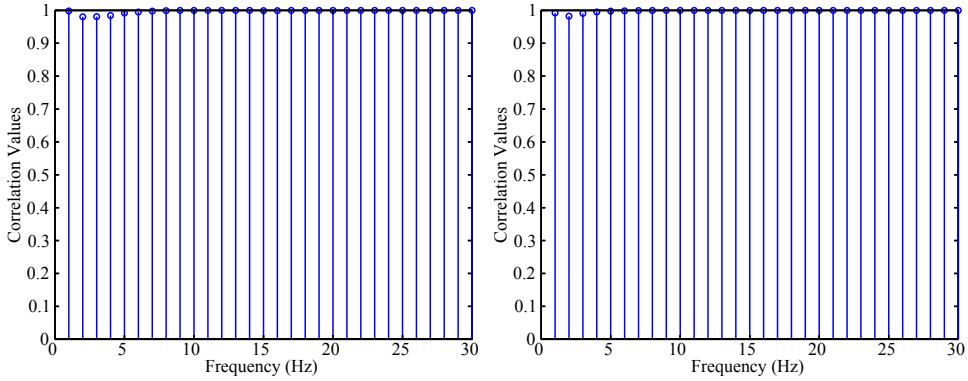

(a) (b)

Figure 6.17: FC of corrected artifact in channel C_3 of a) subject 1 and b) subject 2.

For channel C_4 of both subjects, similar results were obtained, however, with slight differences. Figure 6.18 shows the corrected channel C_4 (red line) and the uncorrected channel C_4 (green line) which results in the same slight correction as channel C_3, however, looking closer, Figure 6.18(a) and 6.18(b) shows that a larger amount of data is corrected comparred to channel C_3 but, it is still considered small correction when comparing channel C_4 to F_z.

Figure 6.19 shows the PSD of both corrected and uncorrected channel which has a peak within the alpha frequency range which indicates motor movement during the recording of the data. Furthermore a larger drop in power is observed between 0 and 10 Hz which is greater than that of channel C_3 but again compared to channel F_z the decrease is small.

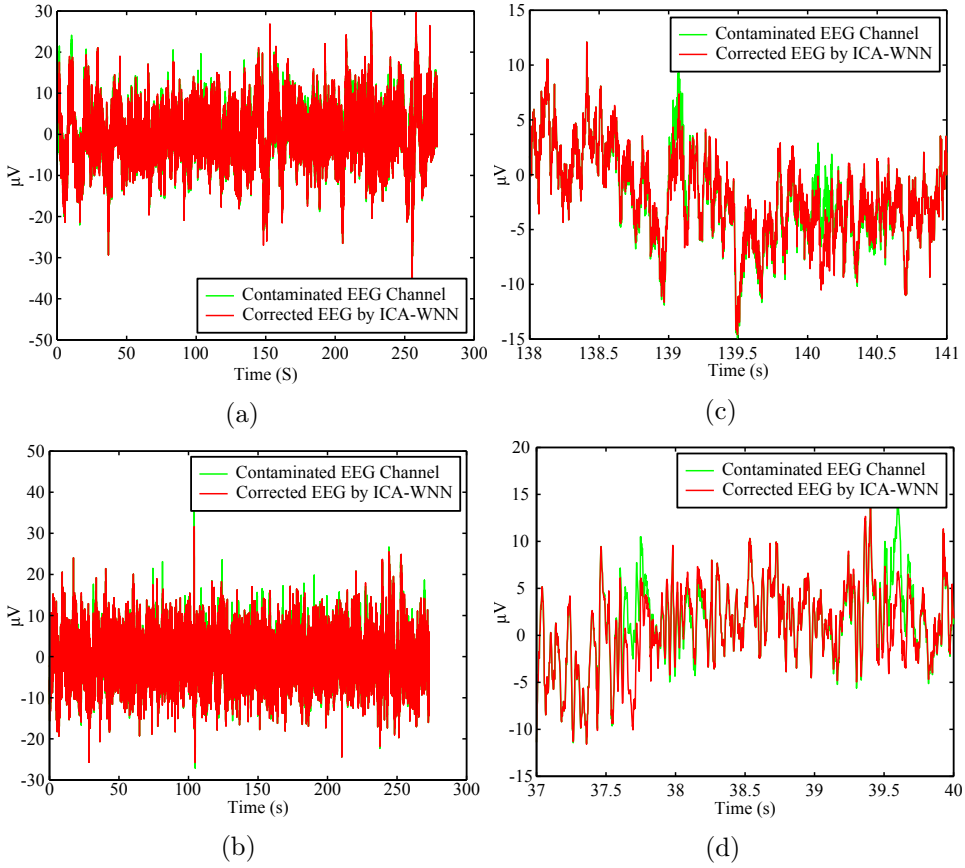

Figure 6.18: Channel C_4 artifact correction of a) subject 1 and b) subject 2 with enlarged views between c) 138 and 141 s for subject 1 and d) 37 and 40 s for subject 2.

The frequency correlation further confirms the results obtained in Figure 6.19. Figure 6.20 shows that for both subjects, between 0 and 10 Hz, a change larger than C_3 occurs.

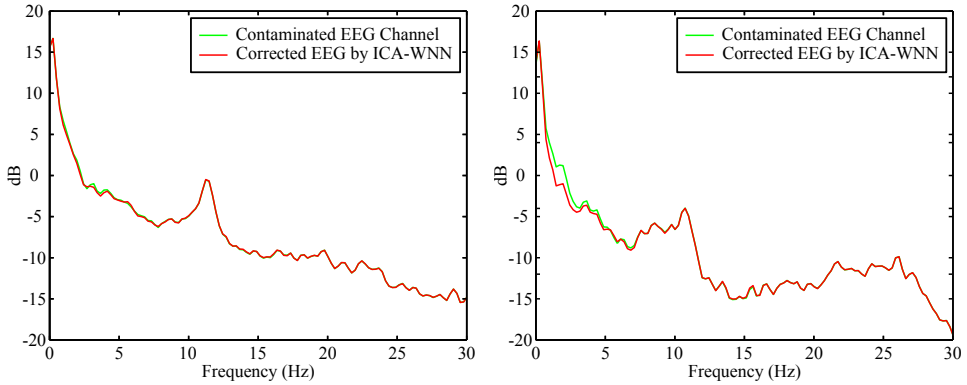

(a) (b)

Figure 6.19: PSD of corrected artifact in channel C_4 of a) subject 1 and b) subject 2.

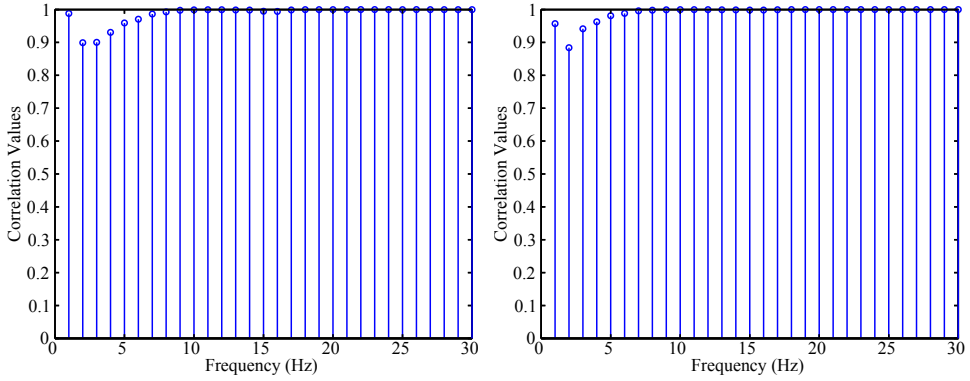

(a) (b)

Figure 6.20: FC of corrected artifact in channel C_4 of a) subject 1 and b) subject 2.

Chapter 7

Discussion

7.1 Successful Results

The accuracy of a process or system that corrects or removes artifacts is dependent on two factors. Firstly the accuracy to which the system can detect the artifact and secondly its ability to either completely remove or correct the artifact. Thus, if each area is proven to have adequate accuracy the overall system or process will produce adequate results.

In order to have an adequate correction system the detection algorithm has to have a high enough success rate. Thus, wavelet analysis having the ability to detect small wave forms with great time resolution is used in conjunction with a threshold value to detect eye blink artifacts. This method is proved successful resulting in an accuracy of 88.2 % for subject 1 and 93 % for subject 2 with an overall accuracy of 90.6 %. Each dataset's threshold was determined manually. However, the accuracy is largely dependent on the individual who determines the threshold (refer to Eq. 5.3.1). If an error is made in determining the maximum amplitude in the eye blinks, the threshold can be incorrect, thus resulting in the eye blink falling short of the threshold. The significance of the blink detection method was to determine how accurately eye blinks can be detected only using a threshold value and wavelet analysis. Achanccaray et al. [62] made use of wavelet transformation, neural networking, and higher order statistics to detect artifacts which resulted in a detection rate of 94.6%. The blink detection algorithm differs with 4 % in accuracy thus, this shows that the wavelet analysis is a powerful tool for artifact detection. The accuracy of the detection algorithm can be further improved by applying higher order statistics and/or neural networks.

Nguyen et al. [15] introduced a combination of wavelet analysis and neural networks which has the ability to decompose a signal into characteristic coefficients as well as the ability to generalize. This study focused on two

WNN models; model 1 correcting only the lowest frequency band and model 2 correcting the three lowest frequency bands of level 8, coif3 decomposition. Both models were trained using eye blink data from only one subject which provided a system requiring very little setup time for each new dataset. Figure 6.1 demonstrates how well a neural network can be trained to correct an eye blink whereas Figure 6.3 demonstrates the generalisation ability of the neural network to correct and eye blink that is different from the training eye blink. For model 1 it is observed that there is still a slight peak which indicates that the artifact was not fully corrected (discussed in the next section) unlike model 2 where the training output is almost identical to the desired output. The frequency content of the signals during training, Figure 6.2, and testing, Figure 6.4, are suppressed, however, it is suppressed more than required. This is caused by the low frequency data still present during the extraction of eye blink artifact causing the WNN to overcorrect low frequency (discussed in the next section) information which confirms the findings of [15]. Nguyen et al. [15] reported that the RMSE achieved for training and testing the WNN resulted in values of 11.2389 and 12.2473 for data samples of 30s and larger. In this study, during training, model 1 produced an RMSE of 8.6605 and model 2 a RMSE of 2.1570, while during testing, model 1 and 2 achieved an average RMSE of 7.7813 and 7.5421 respectively. Both model 1 and 2 demonstrated better accuracy than [15] due to the new structure and level of decomposition of the WNN.

To further improve the eye blink artifact correction and reduce the amount of EEG data lost due to overcorrection of the low frequency band and unnecessary EEG data processing, the blink detection method and WNN is combined with ICA. Independent source components are determined by ICA and only the eye blink artifacts present in the independent source component is processed. The capability of artifact correction was tested on simulated independent source components. Combining blink detection and WNN blink correction successfully corrects only the eye blink artifacts present in the independent source component while the remainder of the signal remains unchanged, as seen in Figure 6.5. From Figure 6.6 it is shown that the corrected independent source component PSD, for both models, is almost identical to that of the artifact free independent source component. By applying the WNN only to the desired area (eye blink artifacts) the remainder of the signal remains unchanged thus retaining most of its low frequency data. The frequency correlation for both models, corrected source component vs. artifact source component (see Figure 6.7(b) and 6.7(d)), indicate that there is a suppression of low frequency data. Figure 6.7(a) and 6.7(c) shows how similar the corrected simulated component is to the artifact free simulated component from which a conclusion can be drawn that the eye blink artifact is corrected however, a miniscule portion of low frequency information is suppressed. The small differences present in the higher frequency bands, 10 to 20 Hz, seen in Figure 6.7(c) and 6.7(d) of model

2 is due to the generalization property of the neural network. Information present in the low frequency bands, which does not require correction, is corrected by the neural network. Model 1 and 2 achieved an average RMSE of 4.0524 and 3.3215 respectively which is less than reported by [15] thus demonstrating the effective correction capabilities of applying WNN to only eye blink artifacts present in the source component. The combined blink detection and WNN blink correction algorithms is not only limited to offline use but can be used for online artifact correction where the combined algorithms is applied directly to a channel rather than an ICA component, similar to the work done by [15].

The simulated data used to test and train both models were simulated at a sampling frequency of 256 Hz. However, not all EEG data is recorded at the same sampling frequency, thus two different datasets were used to test the blink detection and WNN correction capabilities. The motor imaginary data set was recorded at a sampling rate of a 1000 Hz. Both models successfully detected and corrected the eye blink artifacts present in the artifact independent source component, see Figure 6.8, as well as suppressed low frequency information, see Figure 6.9. The frequency correlation, shown in Figure 6.10, further verify the results obtained from the PSD plots which shows low frequency information being suppressed. Model 2, however, did not only supress low frequency data but slightly increased the power of the source component at 15 Hz.

The blink detection data, recorded at a sampling rate of 128 Hz, was also used to determine the correction rate of both models by correcting eye blinks present in the artifact independent source components of 25 sessions. Model 2 showed promising results, obtaining a correction rate of 99.3 % for subject 1, 97.2 % for subject 2, and an overall correction rate of 98.3 %. Figure 6.11(b) and 6.11(d) shows that the eye blink artifact are fully corrected whereas the remaining independent source component is untouched. Model 1, however, only obtained a correction rate of 0.7 % for subject 1, 2.3 % for subject 2, and an overall correction rate of 1.5 %. Figure 6.11(a) and 6.11(c) shows the eye blinks not being fully corrected resulting in a smaller spike like wave that resembles the coif3 wavelet. This phenomenon is caused by the high level of wavelet decomposition which forces the eye blink artifact properties to split between different low frequency bands instead of just the lowest frequency band thus, model 1 only corrected part of the eye blink. The phenomenon can also be seen in Figure 6.1(a) and 6.3(a) where there is still a slight peak remaining. Due to the poor correction rate, model 1 was disregarded for the remainder of the study.

After vigorous testing the complete correction algorithm (ICA, blink detection, and WNN model 2) was applied to a motor movement dataset (sampling

rate 500 Hz) in order to determine whether it can improve EEG signals for BCI applications. The EEG data was decomposed into independent sources and then the source containing eye blink artifacts were corrected and remixed to produce artifact free EEG data. Channel F_z was evaluated, due to its high density of eye artifacts, to determine to what degree the artifacts were corrected. Figure 6.12 shows that the eye blinks are successfully corrected. This indicates that after correcting the artifact independent source component, reintroducing the corrected signal into the source matrix, and reconstructing the EEG, all the channels that were affected by the eye blink artifacts are corrected. Figure 6.13 and 6.14 show that the low frequency data is suppressed indicating some low frequency information being removed however, the power increase at 15 Hz still occurs. It was observed that subject 1 produced slower wave activity than subject 2, which caused the increase of 15 Hz activity to be greater than that of subject 2.

Channel C_3 and C_4 were evaluated to determine the severe impact eye blink artifacts have on electrodes located over the motor cortex. The results obtained from channel C_3 and C_4 were very similar for both subjects. Figure 6.15 and 6.18 demonstrates the corrections that were made by the complete algorithm. However, the corrections are miniscule due to the resistive properties of brain tissue which reduces the amplitude of the eye blink artifacts as it travels throughout the scalp. Figure 6.16 and 6.19 shows the PSD of both the original and corrected signal and confirms the result that miniscule corrections are made. This is shown by the minute decrease in power between 0 and 10 Hz of the corrected signal (red line). The 15 Hz increase in power that is present in channel F_z is not present in either channel C_3 or C_4. The increase in power follows the same mixing properties as the eye blink artifacts thus decreasing with amplitude as it travels through the scalp resulting in a miniscule increase in power at channel C_3 and C_4. The frequency correlation of both subjects for C_3 or C_4, see Figure 6.17 and 6.20, shows that the changes that occurred has slightly changed the data in the frequency domain, however, this change is so small that it does not affect the data. During the recording of the EEG data each individual was instructed to extend their arms and rotate their hands. Motor functions primarily take place in the alpha frequency band (8-13 Hz) thus an increase in power is observed at 10 Hz, see Figures 6.16 and 6.19.

7.2 Problems Encountered

The blink detection algorithm did not detect 11.8 % of subject 1's artifacts, 7 % of subjects 2's artifacts, and overall did not detect 9.4 % of the artifacts present in the trials of the blink dataset. During detection, when two eye blink artifacts are in close proximity of one another, only one will be detected and the other ignored. Occasionally both artifacts will be present in the data

segment because of the extreme close proximity. Instructing the individual taking the test to blink in slow intervals can reduce this phenomenon from occurring. The algorithm can be altered to determine the distance between two artifacts and if that distance is greater than a set threshold the segment window is enlarged to include both eye blink artifacts.

When the WNN corrects a single eye blink artifact, contained in a 1s segment of data, it corrects the eye blink artifact but also overcorrects the low frequency data. During the simulated signal generation, eye blink artifacts are extracted from EEG data by applying a low pass filter which results in only low frequency data remaining, such as the eye blink artifact. The eye blink artifact that is extracted and combined with the simulated artifact free signal still contains some low frequency data. Thus during training, the WNN learns to remove the extracted eye blink artifact with its low frequency data to produce the artifact free simulated signal. Therefore the WNN considers the low frequency data as artifacts. This shows that the accuracy of the WNN is also dependent on how accurately only the eye blink artifact can be extracted. In order to prevent the over correction of the entire signal the WNN is only applied to a small segment of data which reduces the amount of overcorrection taking place.

During the component correction using model 2 it was noticed that a power increase at 15 Hz occurs with the corrected source component. This increase occurs during the segment replacement procedure where the segment in the original signal is zeroed and then replaced with the corrected segment. Because the corrected segment has very little low frequency activity, due to overcorrection, and the original signal has a substantial amount of low frequency data a step like curve is generated between the two points of the original and corrected segment, see Figure 7.1.

For example, the original signal's mean within the segment is below zero where the corrected segment mean is slightly above zero. Thus, inserting the corrected segment will cause a jump from a mean below zero to slightly above zero. This jump can be reduced by readjusting the mean of the corrected signal to replicate the mean of the original signal just before the blink occurs. Thus windows can be used to determine the average mean of the signal before the eye blink occurs and after the eye blink occurs. The mean of the corrected 1 s segment is then adjusted according to the means calculated before and after the eye blink. The readjusted segment is then used to replace the eye blink artifact.

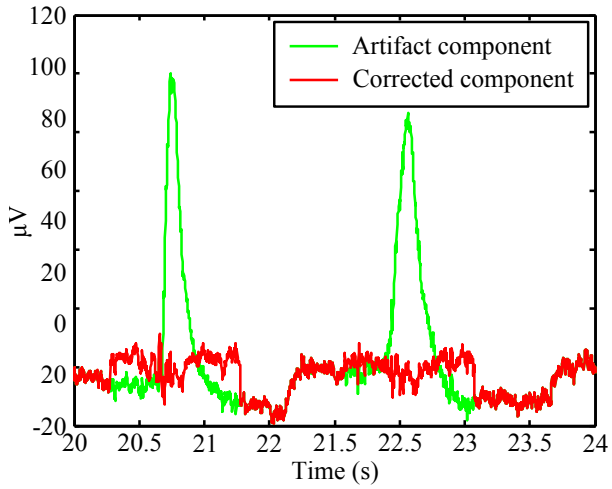

Figure 7.1: Sudden shift in signal mean.

7.3 Future Work

The results obtained is a step in the right direction and can be used to address the problem of eye blink contamination of EEG data. However, there are still some improvements that can be made to improve the current system. The current training method used to train the WNN can be improved by simulating both neural activity and eye blink. This allows the WNN to recognise the eye blink only and no other low frequency data thus reducing the overcorrection of the WNN in the low frequency band. The system manually adjust the threshold for each data set to achieve acceptable results. Incorporating higher order statistics and neural networking can automate this process removing the error caused by the individual determining the threshold as well as removing the need to adjust the setup for every new dataset. The neural network will be trained to detect an eye blink using the coefficients of a wavelet transform as well as statistics. The system only limited to eye blinks can be duplicated and trained to detect and correct eye movement. With two systems trained and tested they can be combined to remove all ocular artifacts from EEG data.

Chapter 8

Conclusion

BCI is a system that allows individuals, who have lost motor function due to ALS, strokes, spinal cord injury, muscular dystrophy, or amputation, a means of interacting with the world by bypassing the neuromuscular channels. The system is directly linked to the brain and uses the neural activity that is manipulated by the individual, to control an external device. The neural activity is acquired through a non-invasive procedure known as EEG which is a popular and cheap recording device able to deliver real time recordings for BCI applications. EEG recording must reflect the true neural activity to ensure an accurate BCI system, however, this is not the case. Unwanted electrical sources are present near the scalp which produces their own electrical activity. These sources' activity are known as artifacts and distort the neural activity of the brain during acquisition.

Out of all the artifacts present, eye blinks are the most encountered artifacts in the BCI system. It is able to distort most of the electrodes recordings found in the frontal lobe due to its amplitude, which is much larger than that of neural activity. Due to this distortion, BCI accuracy is reduced leading to inaccurate classification of tasks. Thus the goal of this study was to develop a novel method of improving EEG signals for BCI classification. The goal was divided into primary and secondary objectives. The primary objectives was to create a method to detect and correct eye blink artifacts where the secondary goal was to determine severity of eye blink artifacts impact on the EEG channels (C_3 and C_4) located above the motor cortex.

A method combining ICA, wavelet analysis, and neural networks was introduced. The independent source components of the EEG data was determined, using ICA, and the artifact source marked. Blink detection was applied to the marked independent source component and the detected eye blinks were exported, in small segments, to the WNN where they were corrected. The detected eye blinks in the artifact independent source component were replaced by the corrected segments and the EEG data was reconstructed producing eye

blink artifact free EEG data.

The blink detection algorithm successfully detected eye blink artifacts with a detection rate of 90.6 %. Both WNN models were trained with simulated EEG data contaminated with extracted eye blink artifacts. Model 1 resulted in an RMSE of 8.6605 for training and 7.7313 for testing where model 2 resulted in 2.1570 for training and 7.5421 for testing. The combination of both blink detection and WNN blink correction applied to the artifact independent source component resulted in a correction rate of 1.5 % for model 1 and 98.3 % for model 2. Due to model 1's poor correction rate it was disregarded for the remainder of the study and model 2 was further evaluated. The combined algorithms, using model 2, successfully removed eye blink artifacts from motor function data. Channel F_z, located on the frontal lobe, showed corrected eye blink artifacts where C_3 and C_4, located over the motor cortex, indicated miniscule change demonstrating that eye blink artifacts barely effects C_3 and C_4.

The significance of this research was to further improve the current processing method in order to minimize the underlying data that is lost during artifact correction. By combining blink detection and the WNN blink correction algorithm the amount of underlying data lost, due to overcorrected low frequency data, is reduced. Combining this with only correcting the artifact independent source component further reduces the underlying EEG data lost. The combination of algorithms moves the research field in removing eye blink artifacts closer to a point where no data is lost during correction. This will help with research regarding the frontal lobe such as investigating emotion [63] and BCI applications such as an individual manipulating the neural activity of the anterior dorsolateral prefrontal cortex, which regulates the flow of information, plans actions, and solve problems to control a cursor [13].

Appendices

Appendix A

Results Obtained During Study

A.1 Eye Blink Detection Results

Table A.1: Eye blink detection results for subject 1.

Sessions	**True number of eye blinks**	**Number of detections**	**Undetected**
1	18	17	1
2	15	13	2
3	15	15	0
4	15	13	2
5	16	15	1
6	17	14	3
7	17	14	3
8	15	11	4
9	14	12	2
10	11	11	0
Total	153	135	18
Detection rates		88.2 %	11.8 %

Table A.2: Eye blink detection results for subject 2.

Sessions	**True number of eye blinks**	**Number of detections**	**Undetected**
1	14	14	0
2	16	15	1
3	14	12	2
4	14	13	1
5	13	11	2
6	17	17	0
7	17	16	1
8	15	15	0
9	16	16	0
10	18	16	2
11	16	15	1
12	15	15	0
13	14	14	0
14	13	13	0
15	18	12	6
Total	230	214	16
Detection rates		93 %	7 %

A.2 Eye Blink Correction Results

Table A.3: Eye blink correction results for subject 1.

Sessions	**Number of detections**	**Number of detections corrected**	
		Model 1	**Model 2**
1	17	0	17
2	13	0	13
3	15	0	15
4	13	0	13
5	15	0	15
6	14	1	13
7	14	0	14
8	11	0	11
9	12	0	12
10	11	0	11
Total	135	1	134
Correction rates		0.7 %	99.3 %

Table A.4: Eye blink correction results for subject 2.

Sessions	**Number of detections**	**Number of detections corrected**	
		Model 1	**Model 2**
1	14	0	14
2	15	0	15
3	12	0	10
4	13	0	13
5	11	0	10
6	17	1	17
7	16	0	15
8	15	0	15
9	16	2	16
10	16	0	16
11	15	0	15
12	15	0	14
13	14	0	13
14	13	0	13
15	12	2	12
Total	214	5	208
Correction rates		2.3 %	97.2 %

References

[1] Wolpaw, J.R., Birbaumer, N., McFarland, D.J., Pfurtscheller, G. and Vaughan, T.M.: Brain-computer interfaces for communication and control. *Clinical neurophysiology : official journal of the International Federation of Clinical Neurophysiology*, vol. 113, no. 6, pp. 767–91, June 2002. ISSN 1388-2457.
Available at: `http://www.ncbi.nlm.nih.gov/pubmed/12048038`

[2] Sanei, S. and Chambers, J.: *EEG signal processing*. 2008. ISBN 9780470025819.
Available at: `http://medcontent.metapress.com/index/A65RM03P4874243N.pdf`
`http://books.google.com/books?hl=en&lr=&id=vIuCV2IKwasC&oi=fnd&pg=PR5&dq=EEG+Signal+`

[3] Liao, L.-D., Chen, C.-Y., Wang, I.-J., Chen, S.-F., Li, S.-Y., Chen, B.-W., Chang, J.-Y. and Lin, C.-T.: Gaming control using a wearable and wireless EEG-based brain-computer interface device with novel dry foam-based sensors. 2012.

[4] Mugler, E.M., Ruf, C.A., Halder, S., Bensch, M. and Kübler, A.: Design and implementation of a P300-based brain-computer interface for controlling an internet browser. *IEEE Transactions on Neural Systems and Rehabilitation Engineering*, vol. 18, pp. 599–609, 2010. ISSN 15344320.

[5] Miranda, E.R. and Brouse, A.: Interfacing the Brain Directly with Musical Systems: On Developing Systems for Making Music with Brain Signals. 2005.

[6] Michel, C.M. and Murray, M.M.: NeuroImage Towards the utilization of EEG as a brain imaging tool. *NeuroImage*, 2012. ISSN 1053-8119.
Available at: `http://dx.doi.org/10.1016/j.neuroimage.2011.12.039`

[7] Teplan, M.: FUNDAMENTALS OF EEG MEASUREMENT M . Teplan. *Measurement Science Review*, vol. 2, pp. 1–11, 2002.

[8] Nunez, P.L. and Srinivasan, R.: Electric Fields of the Brain : The neurophysics of EEG An Overview of Electromagnetic Fields. vol. c, pp. 1–2, 2009.

[9] Li, Y., Ma, Z., Lu, W. and Li, Y.: Automatic removal of the eye blink artifact from EEG using an ICA-based template matching approach. *Physiological measurement*, vol. 27, pp. 425–436, 2006. ISSN 0967-3334.

[10] Jung, T.-P., Humphries, C., Lee, T.-W., Makeig, S., McKeown, M.J., Iragui, V. and Sejnowski, T.J.: Extended ICA removes artifacts from electroencephalographic recordings. In: *Advances in Neural Information Processing Systems*, vol. 10, pp. 894–900. 1998. ISBN 0-262-10076-2.

[11] Repovš, G.: Dealing with Noise in EEG Recording and Data Analysis Spoprijemanje s šumom pri zajemanju in analizi EEG signala. pp. 18–25, 2010.

[12] Li, M.g., Cui, Y. and Yang, J.: Automatic Removal of Ocular Artifact from EEG with DWT and ICA Method. *Applied Mathematics & Information Sciences*, vol. 7, pp. 809–816, 2013.

[13] Vansteensel, M.J., Hermes, D., Aarnoutse, E.J., Bleichner, M.G., Schalk, G., Van Rijen, P.C., Leijten, F.S.S. and Ramsey, N.F.: Brain-computer interfacing based on cognitive control. *Annals of Neurology*, vol. 67, pp. 809–816, 2010. ISSN 03645134.

[14] Venkataramanan, S., Kalpakam, N.V. and Sahambi, J.S.: A Novel Wavelet Based Technique for Detection and De-Noising of Ocular Artifact in Normal and Epileptic Electroencephalogram. pp. 180–183, 2004.

[15] Nguyen, H.-A.T., Musson, J., Li, F., Wang, W., Zhang, G., Xu, R., Richey, C., Schnell, T., McKenzie, F.D. and Li, J.: EOG artifact removal using a wavelet neural network. *Neurocomputing*, vol. 97, pp. 374–389, November 2012. ISSN 09252312.
Available at: `http://linkinghub.elsevier.com/retrieve/pii/S092523121200358X`

[16] Beer, N.A.M.D., Meurs, W.L.V. and Grit, M.B.M.: Educational simulation of the electroencephalogram (EEG). vol. 9, pp. 237–256, 2001.

[17] Fox, S.I.: *Fundamentals of Human Physiology*. McGraw-Hill, New York, 2009.

[18] Weinberg, J. and Krebs, C.: Neuroanatomy Tutorial.

[19] Szachewicz, P.: *CLASSIFICATION OF MOTOR IMAGERY FOR BRAIN-COMPUTER INTERFACES*. Ph.D. thesis, Poznan University of Technology, 2013.

[20] Lopes, F.: EEG: Origin adn Measurement. pp. 19–39, 2010.
Available at: `http://link.springer.com/10.1007/978-3-540-87919-0`

[21] Zinke-Allmang, M.: *Physics for the Life Sciences*. 1st edn. Nelson, Toronto, 2009.

[22] Lee, L., Engineering, E. and Lin, Y.: Basic Principles of Electroencephalography & Magnetoencephalography.

[23] Libenson, M.H.: *Practical Approach to Electroencephalography*. 2012. ISBN 9781455745944.

[24] Forslund, P.: A Neural Network Based Brain - Computer Interface for Classification of Movement Related EEG. , no. December, 2003.

[25] Geodesics, E.: Net Station Acquisition T echnical Manual. Tech. Rep., 2003.

[26] Polytechnique, E. and Lausanne, F.D.E.: *EEG Signal Classification for Brain Computer Interface Applications*, vol. 7. 2002. ISBN 012466606X.
Available at: `http://dsp-book.narod.ru/WVT/BZ.pdf`

[27] Larsen, E.A. and Wang, A.I.: Classification of EEG Signals in a Brain- Computer Interface System. , no. June, 2011.

[28] Menon, V. and Crottaz-Herbette, S.: COMBINED EEG AND F MRI STUDIES OF HUMAN. vol. 66, no. 05, 2005.

[29] Ashrafulla, S.: EEG and MEG : functional brain imaging with high temporal resolution Syed Ashrafulla electrical signals in the brain. 2001.

[30] McFarland, D.J., Sarnacki, W.A., Vaughan, T.M. and Wolpaw, J.R.: Brain-computer interface (BCI) operation: Signal and noise during early training sessions. *Clinical Neurophysiology*, vol. 116, pp. 56–62, 2005. ISSN 13882457.

[31] Manuel, I. and Núñez, B.: Artifact Detection. p. 33, 2010.

[32] Joyce, C.A., Gorodnitsky, I.F. and Kutas, M.: Automatic removal of eye movement and blink artifacts from EEG data using blind component separation. vol. 41, 2004.

[33] Alhomida, A.: Chapter 11: Sweat Fluid.

[34] Goh, S., Ng, S., Phang, Y., Yong, X., Lim, E., Yazed, A. and Shuhaida, Y.: A brain computer interface for control of a prosthetics hand. *Journal of Science and Technology in the Tropics*, pp. 35–41, 2005.

[35] Krusienski, D.J., Sellers, E.W., Bayoudh, S., Mcfarland, D.J., Vaughan, T.M. and Wolpaw, J.R.: A comparison of classification techniques for the P300 Speller. vol. 3, pp. 299–305, 2006.

[36] Al-ani, T. and Trad, D.: Signal Processing and Classification Approaches for Brain-computer Interface. *Intelligent and Biosensors, Edited by Vernon ...*, , no. January, 2010.
Available at: `http://cdn.intechopen.com/pdfs/6798/I...erface.pdf`

[37] Varghese, J.P.: *Analysis of EEG Signals For EEG-based Brain-Computer Interface*. Ph.D. thesis, Mälardalen University, 2009.

[38] Mackay, W.A.: *Wheels of Motion : Oscillatory Potentials in the Motor Cortex*. 2005. ISBN 0849312876.

[39] Ghandeharion, H. and Erfanian, A.: A fully automatic ocular artifact suppression from EEG data using higher order statistics: improved performance by wavelet analysis. *Medical engineering & physics*, vol. 32, pp. 720–729, 2010. ISSN 13504533.

[40] Klados, M.a., Papadelis, C., Braun, C. and Bamidis, P.D.: REG-ICA: A hybrid methodology combining Blind Source Separation and regression techniques for the rejection of ocular artifacts. *Biomedical Signal Processing and Control*, vol. 6, no. 3, pp. 291–300, July 2011. ISSN 17468094.
Available at: `http://linkinghub.elsevier.com/retrieve/pii/S1746809411000061`

[41] James, C.J. and Hesse, C.W.: Independent component analysis for biomedical signals. *Physiological measurement*, vol. 26, pp. R15–R39, 2005. ISSN 0967-3334.

[42] Hyvärinen, A. and Oja, E.: Independent Component Analysis : Algorithms and Applications. vol. 1, no. 1, 2000.

[43] Langlois, D., Chartier, S. and Gosselin, D.: An Introduction to Independent Component Analysis : InfoMax and FastICA algorithms. vol. 6, no. 1, pp. 31–38, 2010.

[44] Koldovcky, Z.: *Fast and Accurate Methods for Independent Component Analysis*. Ph.D. thesis, Czech Technical University, 2005.

[45] Kirkove, M., François, C. and Verly, J.: Comparative evaluation of existing and new methods for correcting ocular artifacts in electroencephalographic recordings. *Signal Processing*, vol. 98, pp. 102–120, 2014. ISSN 0165-1684.
Available at: `http://dx.doi.org/10.1016/j.sigpro.2013.11.015`

[46] Mozaffer, S. and Petr, D.W.: Artifact Extraction from EEG Data Using Independent Component Analysis. Tech. Rep. December, Information and Telecommunication Technology Center, 2002.

[47] Delorme, A., Plamer, J. and Oostenveld, R.: Comparing results of algorithms implementing blind source separation of EEG data. *. . . Foundation and NIH . . .*, 2007.
Available at: `http://sccn.ucsd.edu/ arno/mypapers/delorme_unpub.pdf`

[48] Kumar, P.S., Arumuganathan, R., Sivakumar, K. and Vimal, C.: Removal of Ocular Artifacts in the EEG through Wavelet Transform without using an EOG Reference Channel. vol. 1, no. 3, 2008.

[49] Samar, V.J. and Swartz, K.: Wavelet Analysis of Neuroelectric Waveforms : A Conceptual Tutorial. vol. 60, pp. 7–60, 1999.

[50] Yamamoto, A.: Wavelet Analysis : Theory and Applications. , no. December, pp. 44–52, 1994.

[51] Kiamini, M., Alirezaee, S., Perseh, B. and Ahmadi, M.: A Wavelet Based Algorithm for Ocular Artifact Detection In The EEG Signals. pp. 165–168. 2008. ISBN 9781424428243.

[52] Krishnaveni, V., Jayaraman, S., Aravind, S., Hariharasudhan, V. and Ramadoss, K.: Automatic Identification and Removal of Ocular Artifacts from EEG using Wavelet Transform Department of Electronics & Communication Engineering , PSG College of Technology , Coimbatore - 641 004 India , venimurthyhotmail.com PSG Institute of Medical Scie. *Measurement Science Review*, vol. 6, no. 4, pp. 45–57, 2006.

[53] Basheer, I.A. and Hajmeer, M.: Artificial neural networks : fundamentals , computing , design , and application. vol. 43, pp. 3–31, 2000.

[54] McCulloch, W.S. and Pitts, W.: A logical calculus of the ideas immanent in nervous activity. *The Bulletin of Mathematical Biophysics*, vol. 5, pp. 115–133, 1943. ISSN 00074985.

[55] Ki, O. and Uncuo, E.: Comparison of three back-propagation training algorithms for two case studies. vol. 12, no. October, pp. 434–442, 2005.

[56] Riedmiller, M. and Braun, H.: A Direct Adaptive Method for Faster Backpropagation Learning : The RPROP Algorithm. pp. 586–591, 1993.

[57] Bogacz, R., Markowska-Kaczmar, U. and Kozik, A.: Blinking artefact recognition in EEG signal using artificial neural network. *. . . 4 th Conference on Neural . . .*, 1999.
Available at: `http://www.cs.bristol.ac.uk/Publications/Papers/2000061.pdf`

[58] Donoghue, J., Blankertz, B., Curio, G. and Muller, K.: Boosting bit rates in non-invasive EEG single trial classification by feature combination and multi class paradigm. *IEEE Trans. Biomed. Eng*, 2004.
Available at: `http://scholar.google.com/scholar?hl=en&btnG=Search&q=intitle:Boosting bit rates in non-invasive EEG single-trial classifications by feature combination and multi-class paradigms#0`

[59] MATLAB: *version 8.0.0.783 (R2012a)*. The MathWorks Inc., Natick, Massachusetts, 2012.

[60] Delorme, A. and Makeig, S.: EEGLAB: an open source toolbox for analysis of single-trial EEG dynamics. 2004.

[61] Jung, A.: Statistical analysis of biomedical data. 2004.
Available at: `http://epub.uni-regensburg.de/10168/1/diss-ediss-abgabe.pdf`

[62] Achanccaray, D.R. and Meggiolaro, M.A.: Detection of artifacts from eeg data using wavelet transform, high-order statistics and neural networks d. 2004.

[63] Bos, D.O.: EEG-based Emotion Recognition - The Influence of Visual and Auditory Stimuli. *Emotion*, vol. 57, pp. 1798–806, 2006. ISSN 15582531.
Available at: `http://www.mendeley.com/research/eegbased-emotion-recognition/`